Stochastic Power Management Strategy for In-Wheel Motor Electric Vehicles

by

Mohammadmehdi Jalalmaab

A thesis
presented to the University of Waterloo
in fulfillment of the
thesis requirement for the degree of
Master of Applied Science
in
Systems Design Engineering

Waterloo, Ontario, Canada, 2014

Author's Declaration

I hereby declare that I am the sole author of this thesis. This is a true copy of the thesis, including any required final revisions, as accepted by my examiners.

I understand that my thesis may be made electronically available to the public.

Abstract

In this thesis, we propose a stochastic power management strategy for in-wheel motor electric vehicles (IWM-EVs) to optimize energy consumption and to increase driving range. The driving range for EVs is a critical issue since the battery is the only source of energy. Considering the unpredictable nature of the driver's power demand, a stochastic dynamic programing (SDP) control scheme is employed. The Policy Iteration Algorithm, one of the efficient SDP algorithms for infinite horizon problems, is used to calculate the optimal policies which are time-invariant and can be implemented directly in real-time application. Applying this control package to a high-fidelity model of an in-wheel motor electric vehicle developed in the Autonomie/Simulink environment results in considerable battery charge economy performance, while it is completely free to launch since it does not need further sensor and communication system.

In addition, a skid avoidance algorithm is integrated to the power management strategy to maintain the wheels' slip ratios within the desired values. Undesirable slip ratio causes poor brake and traction control performances and therefore should be avoided. The simulation results with the integrated power management and skid avoidance systems show that this system improves the braking performance while maintaining the power efficiency of the power management system.

Acknowledgements

I would like to thank my supervisor, Professor Nasser Azad for his support and guidance. I am also grateful to Professor K. Ponnambalam and Professor Soo Jeon for providing constructive suggestions and valuable comments on my thesis.

To My Parents and Wife

Table of Contents

List of Figures

List of Tables

Chapter 1

Introduction

1.1 Background

Today, electric propulsion vehicle technologies, such as battery electric vehicle (BEV), hybrid electric vehicle (HEV) and plugin HEV (PHEV), are becoming more and more commercialized and popular. From 487,000 electric propulsion vehicles sold globally in 2012 to 592,000 in 2013, it shows around 23% increase in just one year [1]. Significant increases in the gas price and green-house gas emissions of the conventional internal combustion engine (ICE) vehicles, which caused many environment damages, are the main concerns which lead worldwide costumers to show more interest in those electrified vehicles. Electric motors with regenerative braking capabilities help electric propulsion vehicles have better efficiencies because, firstly, their efficiency is about 75% while ICE efficiency is about 35% due to high heat loss of engines; secondly, electric motors harvest up to 85% of kinetic energy of braking for recharging the batteries; and finally, they reduce idle emissions by turning the engine off and use motor in congestion stop and go situations.

1.1.1 Battery Electric Vehicles

BEV is a promising green transportation technology among electric propulsion vehicles due to no usage of any kind of fossil fuels, and consequently, no greenhouse-gas emissions since it has no engine and all driving torque is delivered by electric motor(s). On the other hand, high initial price of BEVs, low capacity and limited life of today's batteries are the current challenges limiting BEVs broad market presence. However, recent advances in lithium-ion battery technologies, power electronics and controller designs, and, an increase in the number of charge station in cities and highways place BEVs in the center of many attentions [2]. BEV sale growth in 2013 shows a big jump of more than 360% fueled by Tesla Model S EV, Toyota RAV4 EV, Nissan Leaf, Honda fit EV, GM Chevy Spark EV, Ford Focus EV, Mitsubishi I and Smart EV (Table 1-1). The high level perspective of this type of powertrain architecture is shown in Figure 1-1.

1.1.2 In-Wheel Motor Electric Vehicles

One attractive and high-performance type of BEVs is in-wheel motor electric vehicle (IWM-EV) which is powered by two or four electric motors attached to the wheels, instead of one central electric motor, which work independently from each other in two operating modes: driving and regenerative braking.

In Figure 1-2, the architecture of an IWM-EV is depicted whereas f1, f2, r1 and r2 mean front right, front left, rear right and rear right electric motors, respectively. The key components involved in power management problem are in-wheel motors, battery and power management controller.

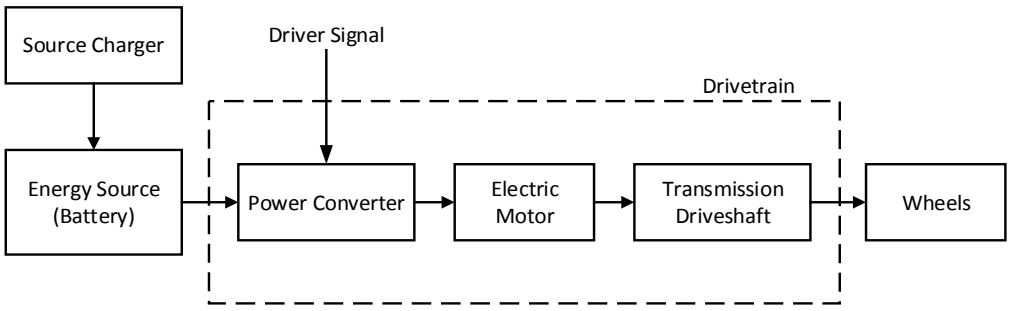

Figure 1-1 High-level architecture of an EV powertrain [3]

Table 1-1 BEV 2013 Sales

BEV	2012 Sale	2013 Sale	%Change
Tesla Model S EV	460	14950	315%
Toyota RAV4 EV	108	915	747.22%
Nissan Leaf	6791	18078	166.21%
Honda fit EV	48	495	931.25%
GM Chevy Spark EV	0	397	-
Ford Focus EV	346	1450	319%
Smart EV	0	603	-
Mitsubishi I	469	1006	114%
Total	8222	37894	360.89%

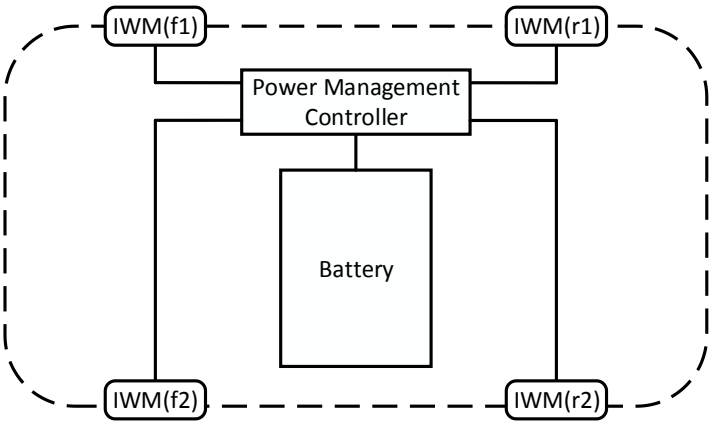

Figure 1-2 A Schematic IWM- EV architecture

IWM architecture improves the controllability and power efficiency of the electric vehicle due to several reasons. Firstly, electric motors are more efficient than ICEs; secondly, electric motors have very fast response, and finally, an IWM-EV has four independent actuators (motors) for driving and braking, and therefore, it has more flexibility to distribute the desired power or regenerative braking between motors in an effective manner. These advantages enable IWM-EVs to perform high performance anti-lock braking and traction control at each wheel, chassis motion control like direct yaw control, and, better estimations of road surface conditions. In addition to these advantages, the compact drivetrains inside the wheels free up space allow the designers to optimize the vehicle layout and presents revolutionary vehicle concepts. Figure 1-3 shows an in-wheel motor's subsystems in detail.

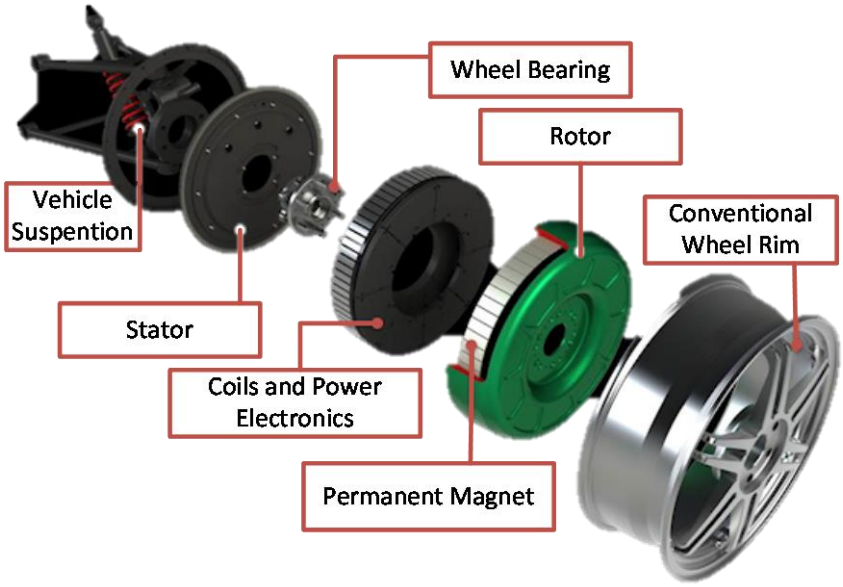

Figure 1-3 Protean In-wheel motor components [4]

© 2014 Protean Electrics

1.1.3 Power Management Problem

One prominent obstacle to wide applications of the BEVs in current stage is the low driving range and slow charge process. Therefore, power management controller, which is a high level vehicle's controller and responsible for efficient driving and decreasing power consumption, receives high degree of importance in BEVs. For BEVs, the power management may contain systems for the reduction of energy expenditure by motors, auxiliary devices such as air conditioner and lighting, wheel slippage reduction, and efficient management of energy sources like the battery and ultra-capacitor. Noticing that the battery is the only energy source of BEVs, it is vital to find more efficient strategies for their energy consumption systems.

The power management for an IWM-EV contains the design of a high-level control algorithm which determines a proper split of the driver's demanded power (P_{dem}) between the in-wheel motors to minimize the battery consumption, while satisfying constraints, such as drivability and stability. An optimal power distribution controller coordinates the motors operation in their high efficiency operating points and causes the minimum battery power consumption. It should be noticed that P_{dem} is specified by the driver pedal commands, therefore, it is function of desired speed and acceleration. Hence, it can be claimed that, in the real-world driving, P_{dem} has a stochastic nature and is not a predetermined set of data.

1.1.4 Stochastic Dynamic Programming (SDP)

The situation and commands in the real-world driving are nondeterministic, thus stochastic strategies are widely studied for the electric vehicles power management. SDP or Markov decision process is one of the most prominent algorithms for optimal control of the stochastic processes:

"Markov decision processes, also referred to as stochastic dynamic programs or stochastic control problems, are models for sequential decision making when outcomes are uncertain. The Markov decision process model consists of decision epochs, states, actions, rewards, and transition probabilities. Choosing an action in a state generates a reward and determines the state at the next decision epoch through a transition probability function. Policies or strategies are prescriptions of which action to choose under any eventuality at every future decision epoch. Decision makers seek policies which are optimal in some sense." [5]

By this compact and rather complete definition from stochastic programming, we can see that the key ingredients of this process are:

1. A set of decision epochs or time steps.
2. A set of system states.
3. A set of available actions for the actuators
4. A set of immediate cost or rewards which are functions of states and/or actions
5. A set of state and action dependent transition probabilities.

We assume that all of these elements are known to the control system at the time of each decision, at every time step, the controller observes the states of the system and chooses an action for the actuators based on the observed states. Every action causes subsequent cost or reward and changes the system to a new state at the next time step or epoch according to a probability distribution. A policy determines how to choose actions in any possible state. The policy generates a sequence of rewards and costs. It is intended by the control designer to find the SDP policy to maximize a function of this reward sequence. One of the possible choices for these functions is the expected total discounted reward or the long-run average reward.

The Markov decision process is a sequential decision model in which, the set of available actions, the rewards, and the transition probabilities, depend only on the current state and action and not on states occupied and actions chosen in the past. The model is sufficiently broad to allow modeling most realistic sequential decision-making problems. Symbolically representation of this sequential decision making model is shown in Figure 1-4.

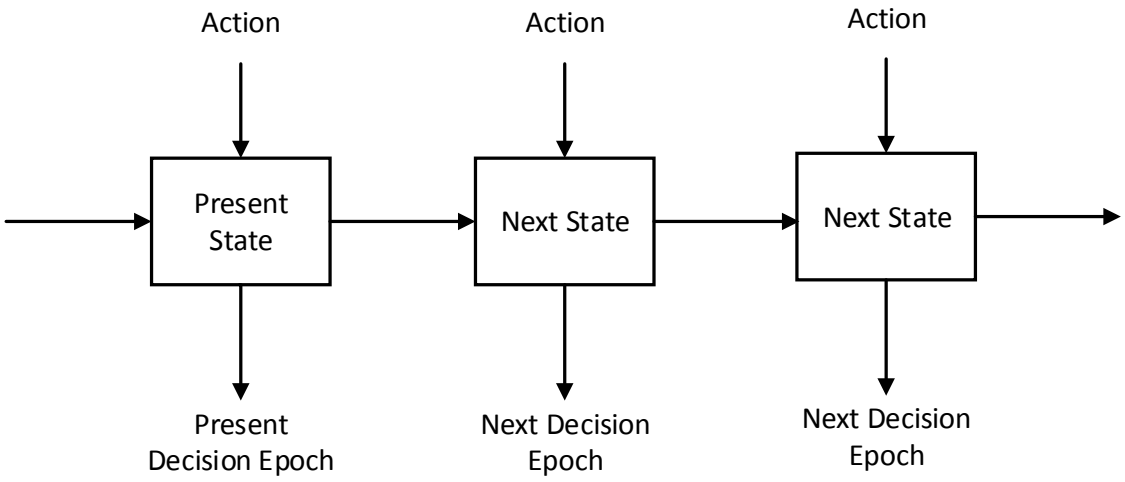

Figure 1-4 Symbolic representation of a sequential decision problem [5]

1.2 Motivation

For deterministic driving scenarios and power demand profiles, Dynamic Programming, DP, is an excellent off-line method to find the optimal solution. But, in the real-world problems, the future driving power demand is uncertain depending on the road traffic, terrain profile, weather, etc. Moreover, the dynamic programming algorithm is highly computational and cannot be used for real-time application during the driving. Thus, we need to implement a method that considers the stochastic nature of the problem and can be used online. To overcome the DP drawbacks, in this study, we propose the use of SDP to resolve the power management problem.

Stochastic power management for the IWM-EVs provides us several advantages in comparison to the other power management methods. First, this control scheme is highly

cost effective since it is free to launch. Despite the intelligent vehicle systems which employ extra sensors and communicating systems to determine future speed profile of the vehicles, SDP only handles past driving information to predict the future situation and does not need extra sensors. Second, SDP rule-base is developed for general real-time application and can be implemented for real-word driving application easily. Third, SDP can handle nonlinear cost functions and constraints seamlessly and we can take advantage of this potential to integrate safety and stability controller, such as skid avoidance and anti-brake systems to the power management strategy.

1.3 Outline

This thesis is organized as follows. In Chapter 2, a review of the literature related to the IWM-EV control and power management is provided. In Chapter 3, a high fidelity model and a control oriented model of the IWM-EV are developed. In Chapter 4, the stochastic modeling of the vehicle power management problem is investigated and the detailed stochastic optimization algorithm is presented. To evaluate the controller, the simulation results and the analyses of the proposed control, methods are given in Chapter 5 followed by the concluding remarks and the future works in Chapter 6.

Chapter 2

Literature Review

This chapter provides an overview of the research literature that constitutes the basis of the thesis. The studied literature focusses on the IWM-EV control and power management. IWM-EV is a BEV in which the electric motors are mounted inside the wheels. In many aspects, IWM-EVs have advantages in comparison with other electric and hybrid electric vehicles, which were discussed in Chapter 1. While there is no commercial IWM-EV currently in the market, many concepts and research vehicle platforms of IWM-EVs have been built and experimented. In section 2.1, some of these models are introduced and evaluated.

The second part of the literature study is the motion control capabilities arising from the IWM-EVs. IWM-EVs are able to perform torque vectoring of left and right wheels and torque distribution between front and rear wheels. These features provide huge maneuverability potentials to the IWM-EVs.

The third part of the literature review is on power management. Power management, or optimal torque/power distribution is the main concern of this thesis. In section 2.3, literature related to the power management problem will be studied. The last part of the literature review is on the application of stochastic dynamic programming to solve vehicle control problem. SDP is a powerful tool to solve nonlinear problems with constraints under uncertainties. The solution of this method can be easily implemented in real time applications.

2.1 Experimental and Concept Models

Recently, several research IWM-EVs have been introduced and evaluated in the literature [6], [7], [8], [9]. These research vehicles are designed by the universities and companies to demonstrate the capabilities and performance of the IWM-EV technology. Besides experimental models, model-based evaluation is a rapid method to investigate the IWM-EVs capability [10].

In [6], it is discussed that in-wheel motors with integrated inverters, control and brakes can be retrofitted to a variety of different vehicles in both pure EV and hybrid configurations such as a sub-compact 3-door C segment vehicle, luxury 4-door sedan, full size pick-up truck, mid-size commercial van. The compact package of IWMs allows the electric drive to be added to every existing vehicle without requiring any significant modification to the vehicle platform and keep the integration costs down.

Yoichi Hori, [7] introduced "UOT Electric March II", shown in Figure 2-1, a novel experimental IWM-EV with four in-wheel motors made for an intensive study of advanced motion control of an IWM-EV.

"C-ta" is an ultra-high-efficient electric commuter concept car developed in (Figure 2-2 and Figure 2-3) [8]. Light and efficient design of this IWM-EV helped it to achieve ultra-low charge consumption of 25.3 km/kWh and acceptable cruising distance of 125 km on a single charge with a little battery of 5 kWh capacity. The electronic control unit (ECU) utilized in this study consists of a real-time operating system (OS) and a FPGA to control the speed and torque distributions. The task of torque distribution between in-wheel motors in the vehicle is assigned to the real-time OS.

In [10], the ADVISOR package, a MATLAB/Simulink based simulation program for rapid analysis of the performance and fuel economy of light and heavy-duty vehicles, is used to simulate an IWM-EV performance and investigate the chassis control systems, such as traction control, electronic differential control, direct yaw moment control and regenerative braking control systems. The results indicate that the performances of the four IWM-EV are significantly improved owning to the application of the innovative architecture of motors and advanced control systems.

In [9], the authors' laboratory developed a completely original IWM-EV which has active front and rear steering systems and high-torque direct drive in-wheel motors in the all wheels. In this paper, the main features of this vehicle are briefly introduced and the studies on pitching control, slip-ratio control and yaw-rate and slip-angle control with lateral force sensors are explained with experimental results.

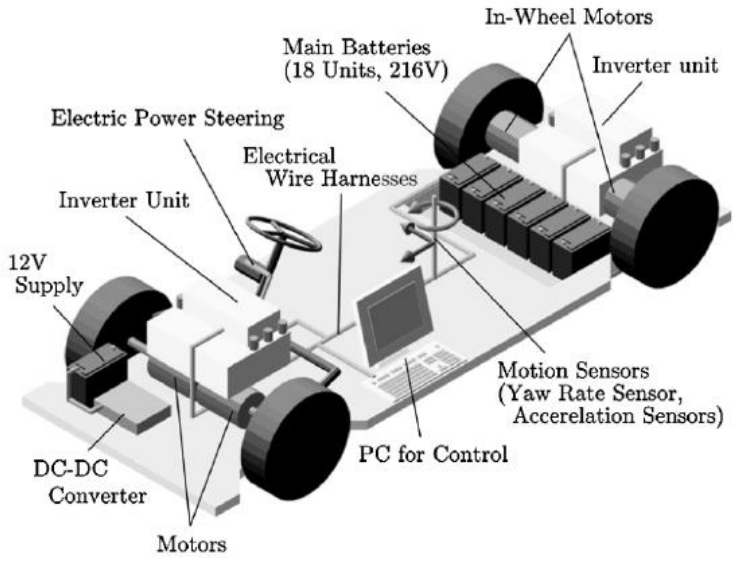

Figure 2-1 UOT Electric March II [7] © 2004 IEEE

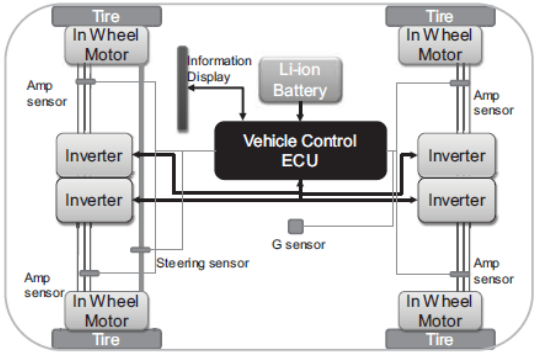

Figure 2-2 C-ta Layout of components

[8] **© 2011 SAE International**

Figure 2-3 Concept Car "C-ta" [8]

© 2011 SAE International

2.2 Control and Dynamic Performance

There are many studies, such as [9], [11], [12], [13], [14], [15], [16], [17], [18], [19] and [20] that take advantage of fast and accurate torque response and torque-vectoring capabilities of IWM-EVs to improve the performance of this type of electric vehicles in terms of the maneuverability, handling and stability.

Jacobsen [11] studied the active safety potential of passenger cars with the IWMs at the rear axle. A mathematical analysis is done, employing a modified bicycle model. The maximum yaw moment limits are investigated for two driving situations, entering the curve and lateral translations and compared the vehicle with traditional wheels. As a result, the time delay of reaching the steady-state yaw speed while entering a curve reduced down to 30 percent, and the maximum lateral acceleration increased by approximately 40 percent, while the results are independent of the vehicle longitudinal speed.

In [12], [20] and [19], the performance of motion control strategies for IWM-EVs, including optimal dynamic traction force distribution and direct yaw moment control (DYC), were studied. In [12], this investigation is done experimentally using two electric vehicles, and the dynamic distribution control is proposed to resolve the actuator redundancy. The experimental results using DYC clearly showed an improvement in the vehicle handling and stability.

In [17], the body slip angle is estimated by making use of the important merit that electric vehicle's motor torque can be measured and controlled accurately. W. Kim and K. Yi [18] developed traction and braking force controller to enhance turning performance of electric vehicle equipped with in-wheel motors.

Lin et al. [13] investigated the effects of IWMs on the unsprung mass of the vehicle and the impact on the vehicle performance and comfort, and proposed a method of attaching the motor to the wheel through springs and dampers exclusively. It is verified that the vibration of EVs with suspended-motor motorized-wheel is similar to EVs with detached-motorized wheels.

De Novellis et al. [14] employed a control allocation algorithm to enhance the handling of a four-wheel-driven fully electric vehicle with individually controlled motors, and analyzed the alternative cost functions developed for the allocation. As a result, the cost functions, based on minimizing the tire slip, led to better control performance than the functions based on the energy efficiency for the case-study vehicle.

K. Jalali et al. [15] developed an advanced torque vectoring controller to generate the required corrective yaw moment through the torque intervention of the individual in-wheel motors to stabilize the vehicle during both normal and emergency driving maneuvers. Novel algorithms were developed for the left-to-right torque vectoring control on each axle and for the front-to-rear torque vectoring distribution action, and several maneuvers were simulated to demonstrate the performance and effectiveness of the proposed advanced torque vectoring controller, and the results were compared to those obtained using an ideal genetic fuzzy yaw moment controller. At the end, the advanced torque vectoring controller was implemented in a hardware- and operator-in-the-loop driving simulator.

2.3 Power Management Strategies

Despite of HEV power management problems which have been widely studied IWM-EVs, power management research is relatively an open area. Traditional EVs have no

choice to manage its energy flow because it has only one traction motor, but IWM-EVs have multiple power source, hence the power management strategy becomes important. A good review on the current IWM-EV power management strategies is presented in [21].

Power management based on the efficiencies of the IWMs are presented in of [22] and [23]. Gu et al. [23] investigated the energy efficiency optimization problem of an electric vehicle driven by four IWMs by developing a comprehensive energy efficiency model of the permanent magnet synchronous motor including the inverter. It is concluded that, to maximize the energy efficiency, for a fixed torque distributor controller, in all driving or braking conditions, the total demanded torque should be distributed evenly between IWMs for EVs driven by permanent magnet synchronous motors. The vehicle test results show that the energy efficiency of the evenly distributed torque control is higher than the control strategy proposed by the control allocation in the literature.

Qian [24] proposed an energy management strategy which is derived by one time step optimization of the front and rear motor torques for given total torque demands. The simulation results validate the proposed strategy since it can save up to 27.4% in the UDDS cycle was compared with a traditional EV. The optimal power split derivation procedure is shown in Figure 2-4.

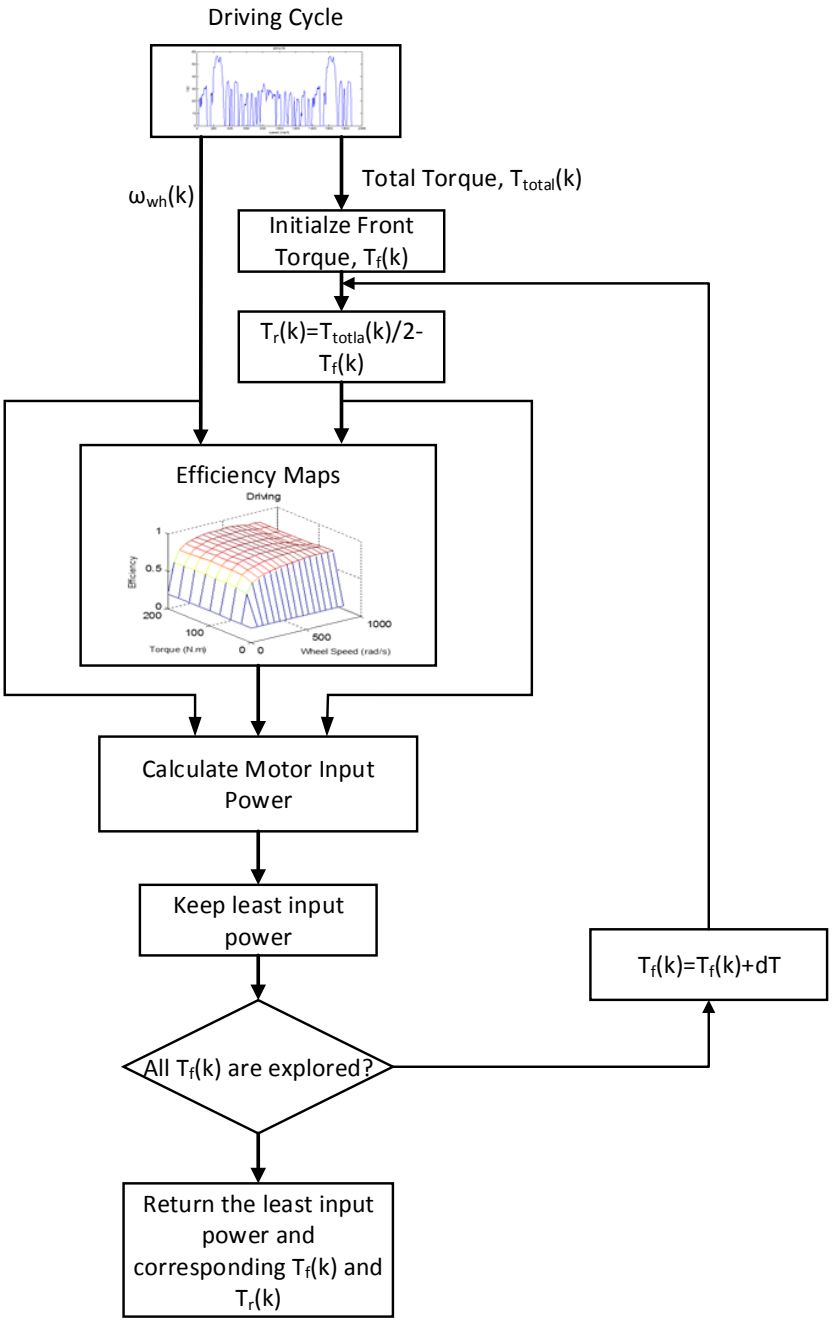

Figure 2-4 Optimal driving torque distribution strategy [24]

Chen [25] presented an energy optimization method for IWM-EVs based on terrain profile preview for a constant speed driving cycle by using dynamic programming to obtain the global optimal energy point for the front-rear torque distributions. The optimization results showed that terrain profile changes the optimal torque distributions and energy savings. For small slope angle terrains, up to 28.9% energy consumption improvement is achieved, while for larger slope angle terrains, this number is around 5%.

K. Maeda et al. [26] developed a four-wheel driving force distribution method based on driving stiffness and slip ratio estimation. Since vehicle velocity measurement by sensors is not fast enough, driving stiffness and slip ratio estimation is applied. Due to the slip ratio estimation, vehicle velocity sensor is not needed and the distribution speed becomes faster. At the end, the authors show the effectiveness of their proposed method experimentally.

In [27], a nonlinear model predictive controller, NMPC, for the regenerative braking control of lightweight IWM-EVs was presented. The proposed controller not only improves the energy recovery of the regenerative braking by determining the front and rear braking torques independently, but also prevents the wheel locks during deceleration when the tire–road friction coefficient is low. The battery power consumption power is included in the cost function to be minimized while the longitudinal slip ratio is considered as the hard constraint to maintain the safety objective. The simulation results, based on a vehicle model in CarSim®, showed that the proposed NMPC has a good vehicle-speed-tracking performance, and it is capable of restoring considerably more regenerative braking energy than a conventional linear controller with a feed forward term and another nonlinear model predictive controller with no consideration of the energy recovery.

Chen et al. [28] presented an energy management system, EMS, for a IWM-EV for a certain trip with terrain preview based on the operating efficiencies of in-wheel motors and a traffic model. The optimal vehicle velocity and globally optimal in-wheel motor actuation torque distributions are simultaneously obtained to minimize the IWM-EV energy consumption by employing the dynamic programming method.

Torque vectoring control strategies for the IWM-EVs which minimize the energy consumption by determining optimal slip ratio for wheels were proposed in [29] and [30]. In [29], a controller is designed to ensure that the slip ratio of each wheel is limited by the optimal value. In [30], the battery power depletion relation, as the function of wheels slip ratios and force distribution ratio, k_{opt}, is derived and differentiated to find the k_{opt}, which makes the battery charge deletion minimized:

$$k_{opt} = \frac{N_r}{N_r + N_f} \tag{2-1}$$

The control allocation is another power management algorithm which is for distributing the desired total control effort among a redundant set of actuators of an over-actuated systems while energy-efficient control allocation strategies for IWM-EV's motion control are proposed in [31], [32], [33], [34] and [35]. This problem is optimized globally by a Karush-Kuhn-Tucker (KKT)-based optimization algorithm in [34]. In [35], an adaptive energy-efficient control allocation (A-EECA) is developed for the planar motion control of IWM-EVs which was low computational cost. In all of these studies, torque distributions are developed based on the IWMs efficiency maps.

Y. Chen and J. Wang [36], developed and compared three different IWM-EV power distributions pattern for normal cornering and circling maneuvers:

1. Front power assignment
2. Rear power assignment
3. All wheel power assignment

Through both simulation and experimental results, it is showed that the three different power distribution methods achieve almost the same vehicle performances in terms of the vehicle sideslip angle, yaw rate and trajectory. Moreover, when a power distribution method is applied to only one pair of wheels, i.e., either the front or rear pair, the other pair of wheels can be utilized to estimate the vehicle longitudinal speed and yaw rate and consequently generate the reference wheel speeds for the wheels. Both simulation and experimental results validate the designs of the three power distribution pattern.

2.4 Stochastic Dynamic Programming

SDP has been extensively studied in the literatures since it can handle constrained nonlinear optimization problems under uncertainties [37]. This strategy has been used for optimal EMS in HEVs [38] and PHEVs [39] to find the optimal power-split between engine and motor. Because of different dynamic and architecture of IWM-EVs, we studied and evaluate this method in this thesis.

H. Zhang et al [40] studied the optimization problem of power management in plug-in hybrid electric vehicles (PHEVs) subject to uncertain and dynamical driving cycles. A stochastic driving cycle model is presented in this paper and the finite-horizon SDP is

utilized to globally optimize vehicle performance in stochastic sense. Simulation results show that the proposed strategy makes a significant progress in improving fuel economy.

D. F. Opila et al. [41] studied power management controllers designed using shortest path stochastic dynamic programming (SP-SDP). The controllers are evaluated on Ford Motor Company's highly accurate proprietary vehicle model over large numbers of real-world drive cycles, and compared to a controller developed by Ford for a prototype vehicle. Results show that the SPSDP-based controllers yield 2-3% better performance than the Ford controller on real-world driving data with even more improvement on a government test cycle. In addition, the SPSDP-based controllers can directly quantify tradeoffs between fuel economy and drivability.

Stochastic drive cycle generation is a necessary tool to evaluate stochastic power management strategies. V. Schwarzer [42] presented a methodology to generate drive cycles based on probabilistic driving profiles. The described approach can be utilized for the stochastic optimization of an energy management controller, EMC, for EVs. The introduced method is implemented in a drive cycle generation tool, and the approach is validated using a model of a parallel HEV powered by fuel cells. Simulation results are presented and the advantage of the proposed method over conventional approaches is proven.

Chapter 3

IWM-EV System Modeling

In this chapter, the IWM-EV models, utilized for design and evaluation of the stochastic power management strategy, are developed and explained as high fidelity model and control-oriented model.

High fidelity model, which is explained in subsection 3.1, is an accurate and detailed representation of IWM-EV and includes validated models of motors, braking system, battery, tires, chassis and driver. To have a reliable evaluation, the performance of designed control strategy should be tested by a high fidelity model of vehicle which is similar to the real vehicles as much as possible. In this study, an experimentally validated high fidelity BEV vehicle model from the Autonomie software is utilized, and modified to have the desired baseline vehicle model. Additionally, high fidelity model is used to validate the control-oriented model, and to do the sensitivity analysis as well as to study the effect of each vehicle's state of the power management solution.

The process of parameter optimization of devised control strategy (SDP) is a highly iterative process, thus high fidelity models cannot be used in this process since they are complex and computationally expensive to run. The control-oriented model, built in subsection 3.3, is a simple and fast model which is accurate enough to characterize the system with the most prominent states of the vehicle from controller point of view.

The parameters of both high fidelity and control-oriented models are from a baseline IWM-EV introduced in [25]. Baseline IWM-EV parameters are listed in Table 3-1. Although the design and the evaluation procedures are done for a specific baseline vehicle, the algorithms presented in this thesis are general and can be implemented in every IWM-EV

Table 3-1 Baseline Vehicle Parameters [25]

SYMBOL	PARAMETERS	VALUES
M	Vehicle Mass	800 kg
$\boldsymbol{E_{bat,max}}$	Battery Capacity	200 Ah
$\boldsymbol{V_{bat}}$	Nominal Voltage of one cell battery	3.3 V
$\boldsymbol{N_{bat}}$	Number of battery cells in series	22
$\boldsymbol{P_{motor}}$	In-wheel motor max power	7.5 kw
A	Vehicle front area	1.66 m^2
$\boldsymbol{\rho}$	Air density	1.2 $\frac{kg}{m^3}$
L	Vehicle wheelbase	1.84 m
$\mathbf{L_f}$	front wheelbase	0.92 m
$\mathbf{L_r}$	rear wheelbase	0.92 m
$\boldsymbol{h}$	Height of center of gravity	0.6 m
$\boldsymbol{R_{eff}}$	Tire effective radius	0.33 m
$\boldsymbol{T_{brake}^{regen,\max}}$	Maximum Regenerative Braking Torque	80 Nm
$\boldsymbol{\mu_{max}}$	Maximum Friction Coefficient	0.8

3.1 High Fiedelity Model (Numerical Model)

High fidelity vehicle model, or numerical model, consists of extract lookup tables or math models for vehicle subsystems which have been developed by accurate experiments in various conditions and driving scenarios. Therefore, several modeling software packages have been developed to provide high fidelity vehicle models for researchers and designers.

The Autonomie is a software environment, developed by Argonne National Lab, to design and evaluate vehicle models in a simulated environment. It includes many pre-built vehicle systems models, thus it enables users to simulate their desired models simply and seamlessly. The software automatically builds a Simulink-based vehicle model and solves the state equations by using the Simulink solver [43],[44].

Although there are many pre-defined models in Autonomie, there is no IWM-EV architecture currently (Autonomie1210). Among the pre-defined models in the Autonomie models library, the nearest models to the IMW-EV architecture are the BEVs default models. To capture the key feature of an IWM-EV, the Autonomie's BEV model should be modified to contain multiple power sources, i.e., electric motors. The operation of modification of the Autonomie's predefined BEV model to an IWM-EV model is done in the Simulink® environment where we added another electric motor to the model. Since all states of the right and left wheels in a straight road driving are the same, four motors of the IWM-EV are simplified to two motors to assign one motor for the front wheels and one motor for the rear wheels. Figure 3-1 shows the default BEV model which is available in the Autonomie environment. Figure 3-2 shows the IWM-EV model modified in the Simulink environment.

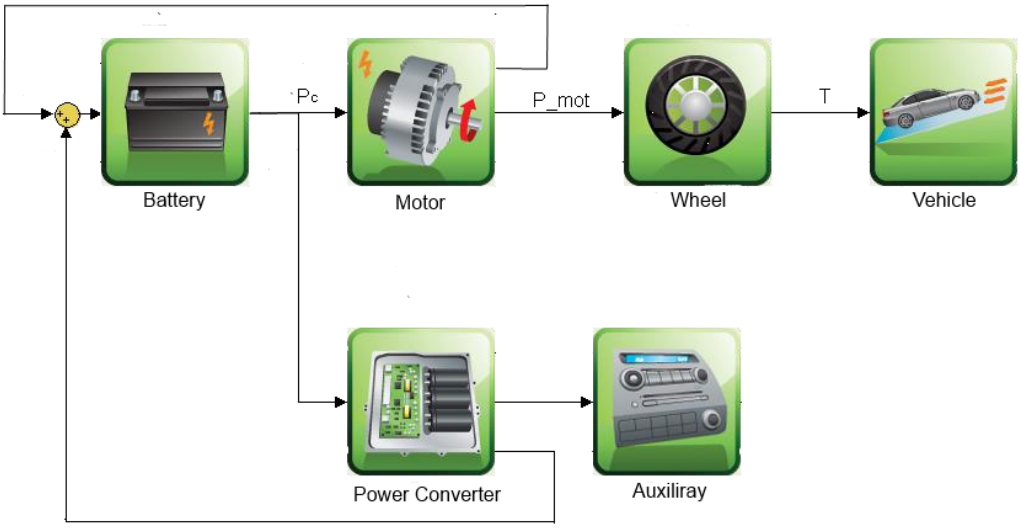

Figure 3-1 High Fidelity Autonomie Model, before modification

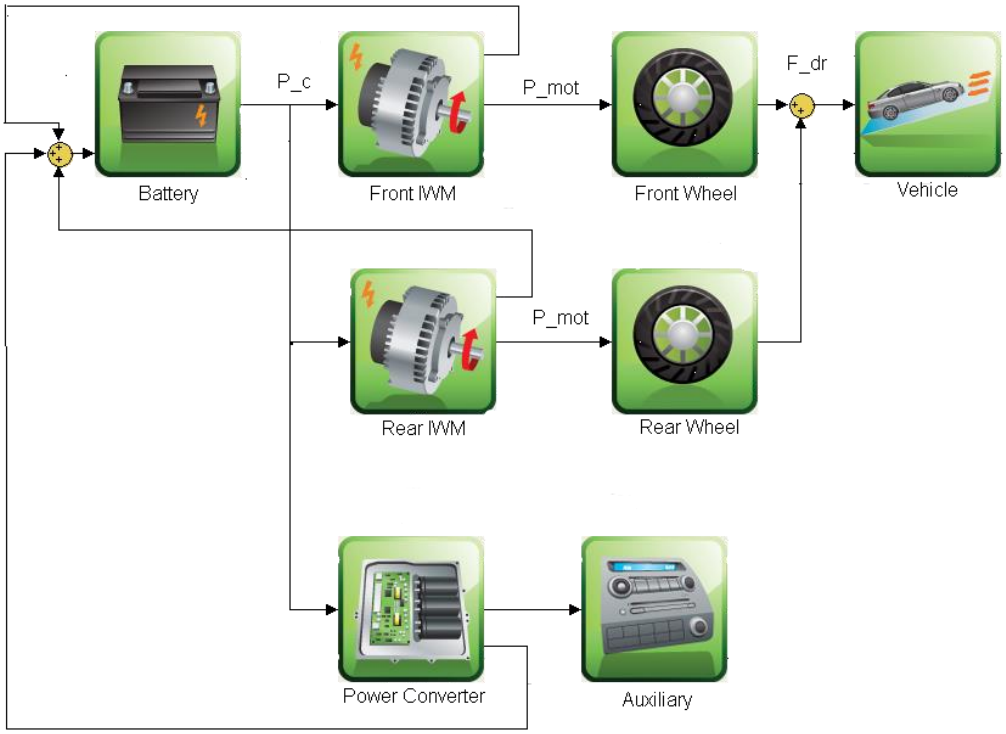

Figure 3-2 High Fidelity Autonomie Model, after modification

From Figure 3-1 and Figure 3-2, we can see that the high fidelity vehicle model consists of:

1. battery block
2. IWM block
3. Wheel block
4. Chassis block

The Battery model contains 72 battery cells. A battery cell block model is shown in Figure 3-4. Inside the battery cell block, the battery cell voltage, V_{cell} is calculated by utilizing lookup-tables for SoC-V_{cell}, SoC-Ohmic resistance and SoC-Polarization resistances. The current polarization is also considered in this high fidelity model of the battery. Figure 3-5 depicted the V_{cell} calculation block, and the experimental relation of the SoC-V_{cell} is demonstrated in Figure 3-3.

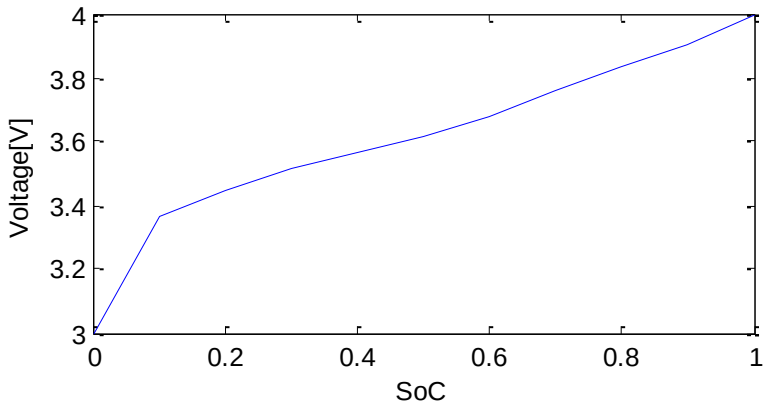

Figure 3-3 $SoC - V_{cell}$ profile

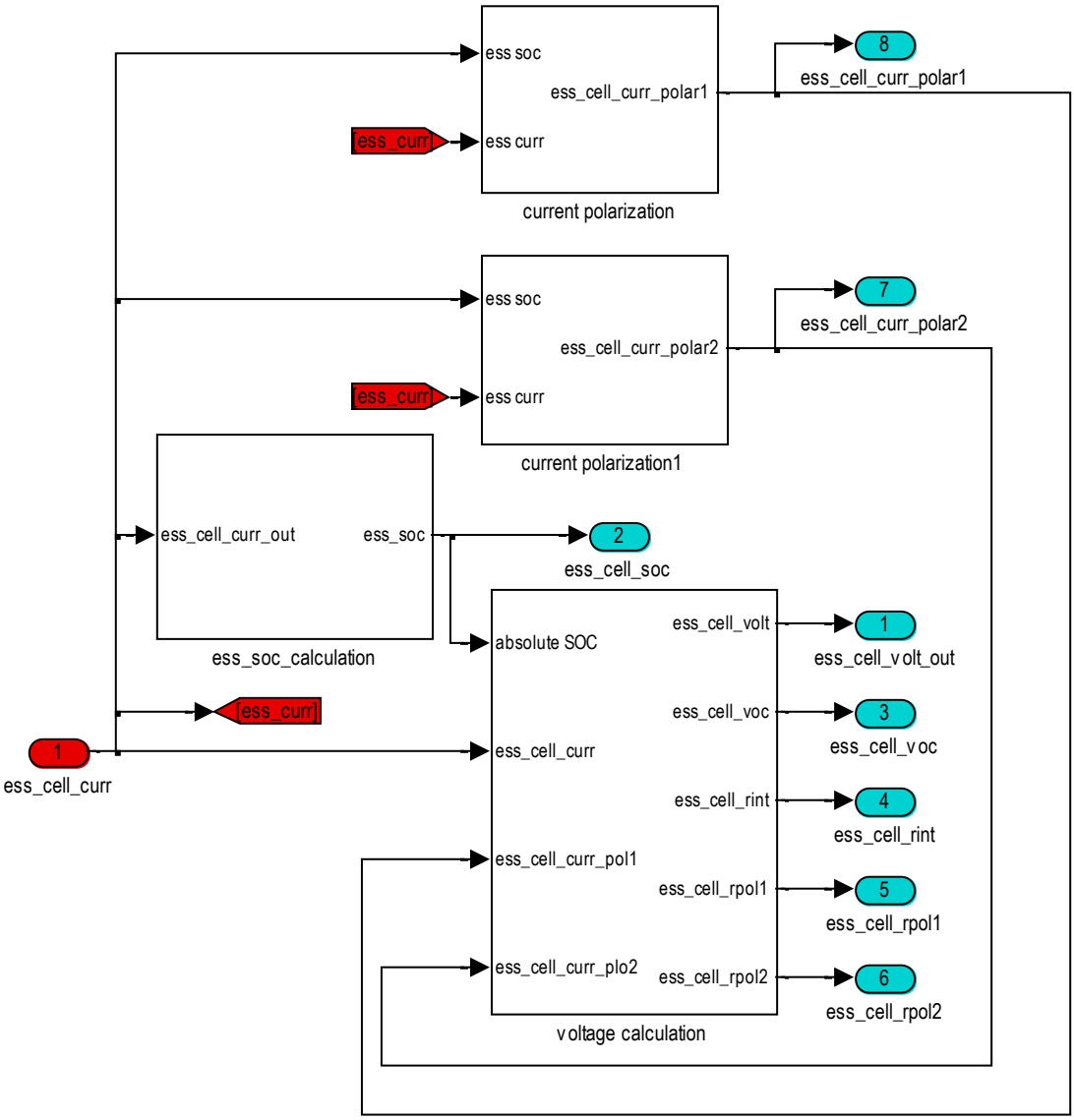

Figure 3-4 Battery cell block

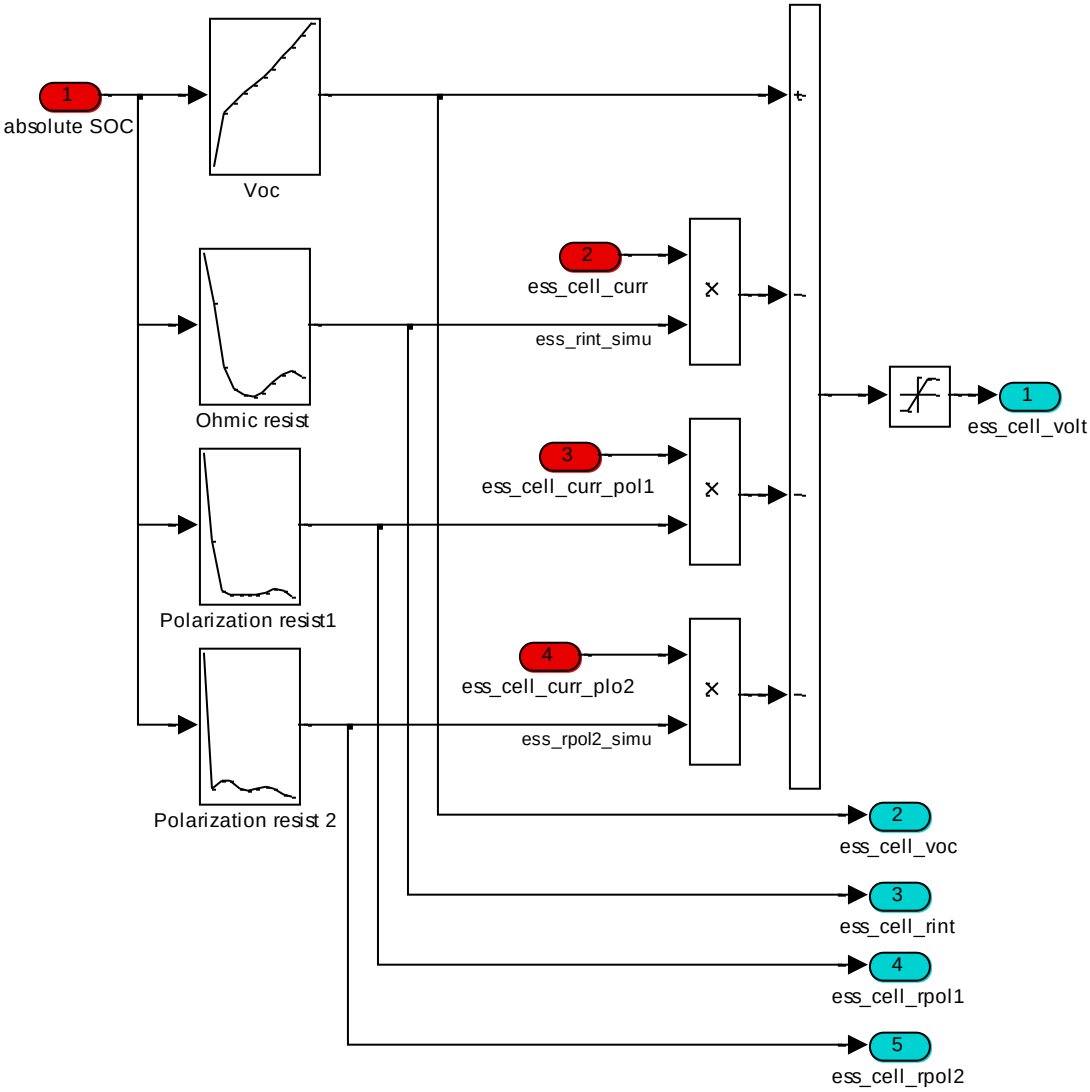

Figure 3-5 V_{cell} calculation block

The IWM subsystem in this modeling package is shown in Figure 3-6. The subsystem mainly consists of the efficiency maps for driving and regenerative braking as shown by gray color in the block. These efficiency maps are shown in Figure 3-7. This IWM model determines the maximum continuous and instantaneous torque based on the rotational speed and heat index to saturate the commanded torques before applying to the wheels (Figure 3-8).

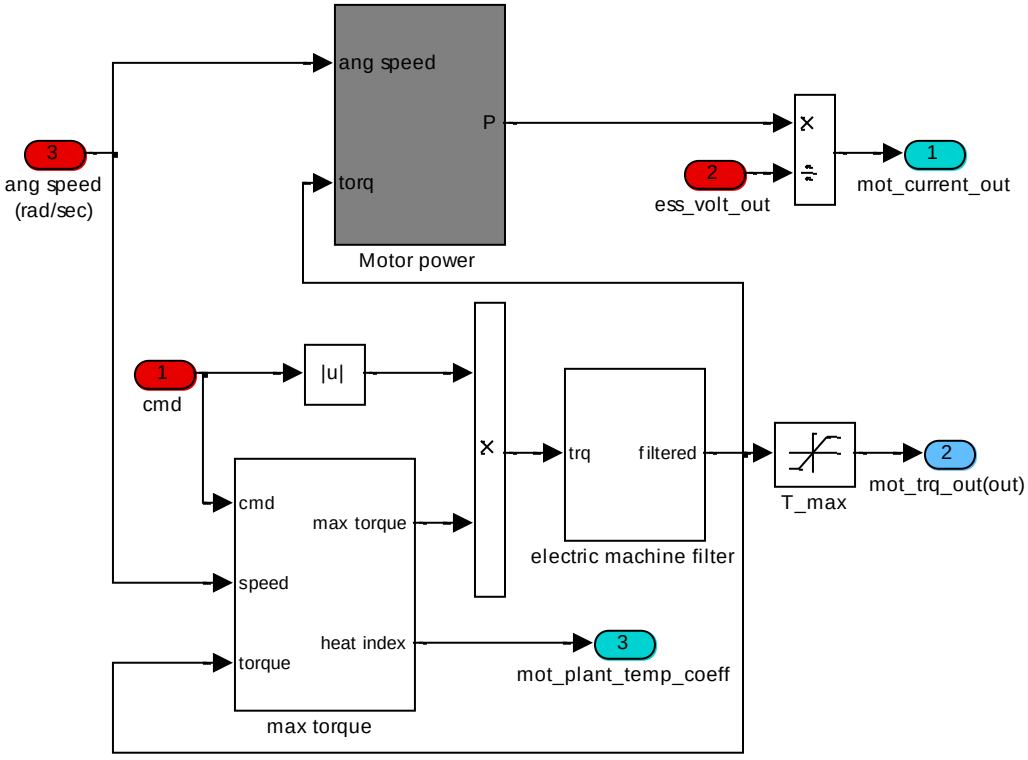

Figure 3-6 IWM model block

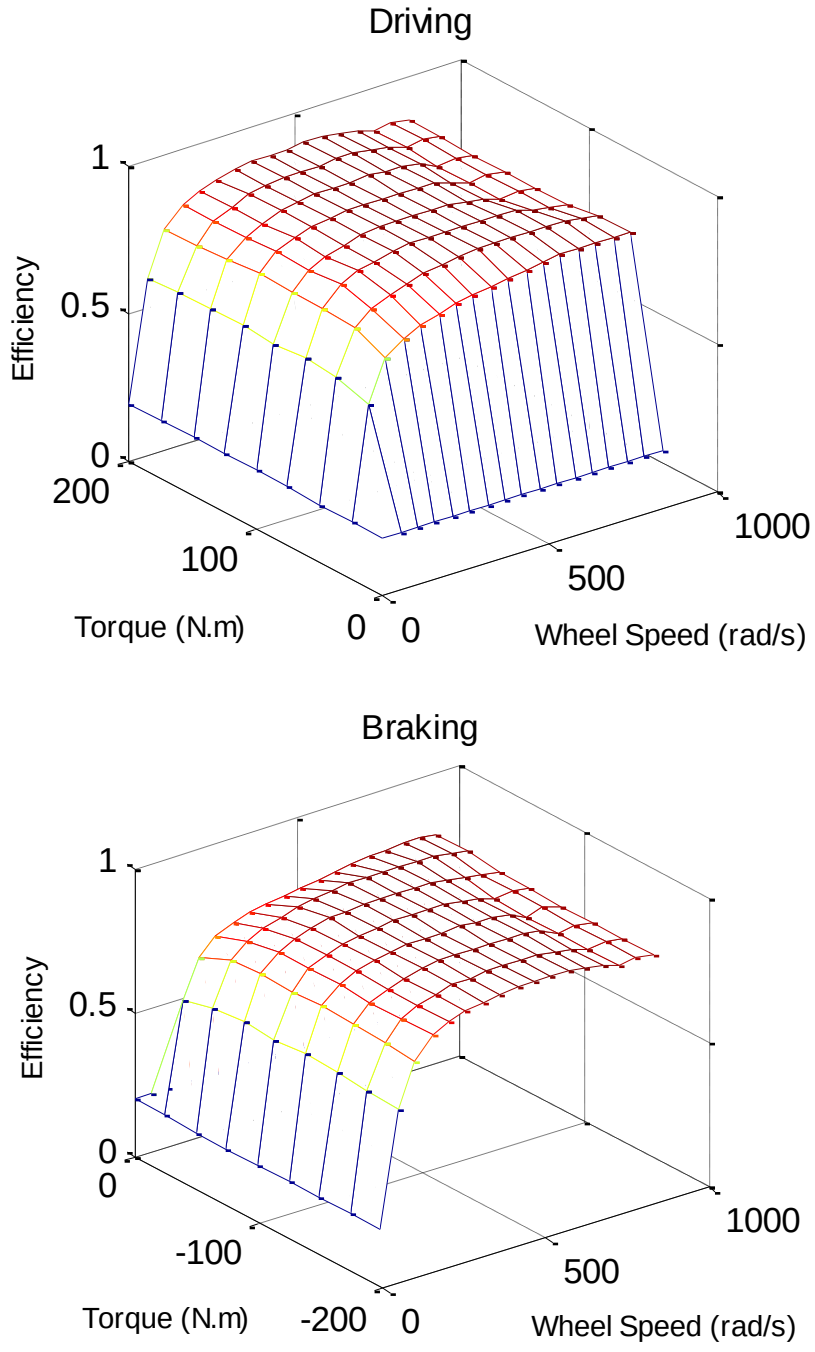

Figure 3-7 Motor efficiency maps for (a) driving (b) braking

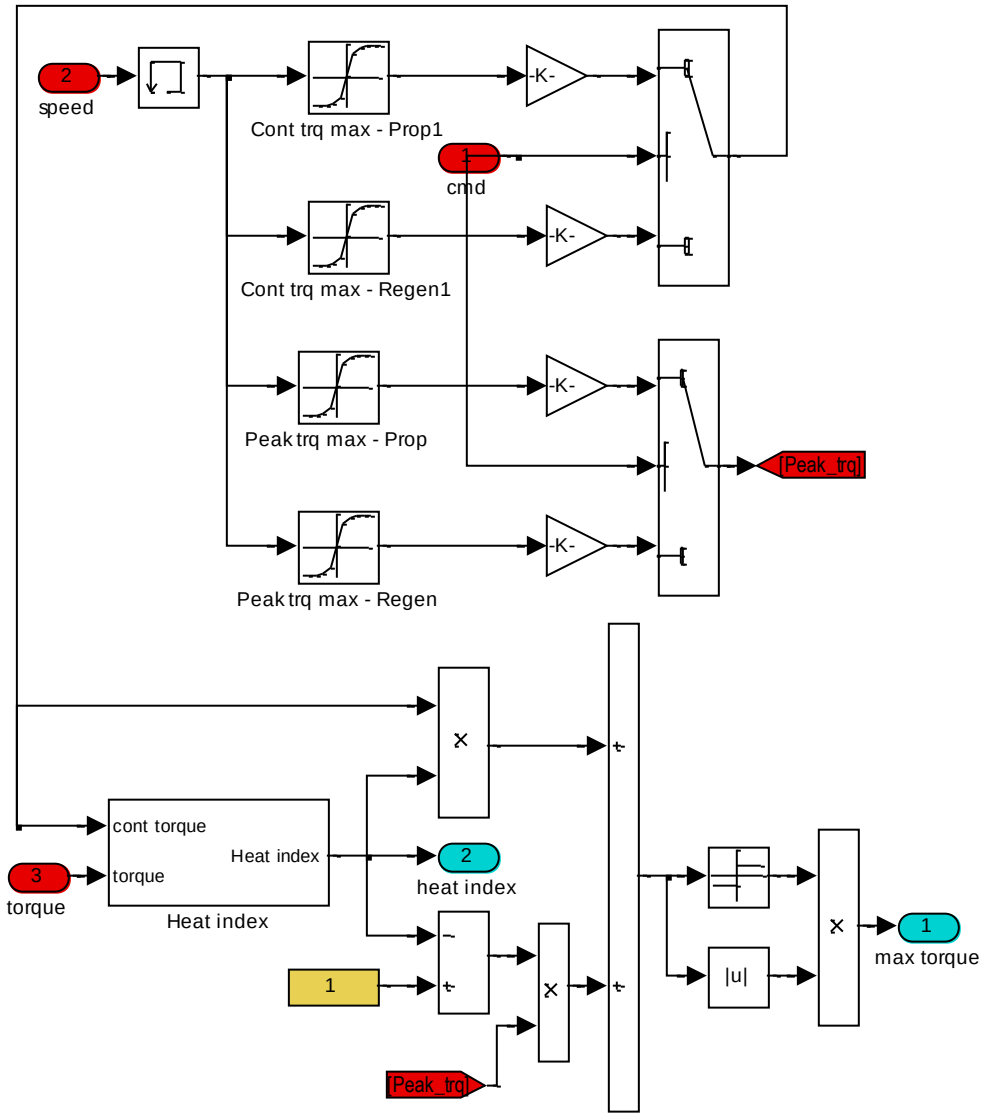

Figure 3-8 Maximum torques determination block for driving and regenerative braking

The original wheel block, obtained from the Autonomie model, simplifies the rotational acceleration equation and assumes that the rotational speed is equal to vehicle speed divided by the effective radius of the wheel. Since we need the exact model of the rotational speed to calculation the slip ratios, we modified the wheel model and consider the rotational acceleration equation which is introduced in equation (3-11). The modified wheel model is depicted in Figure 3-9.

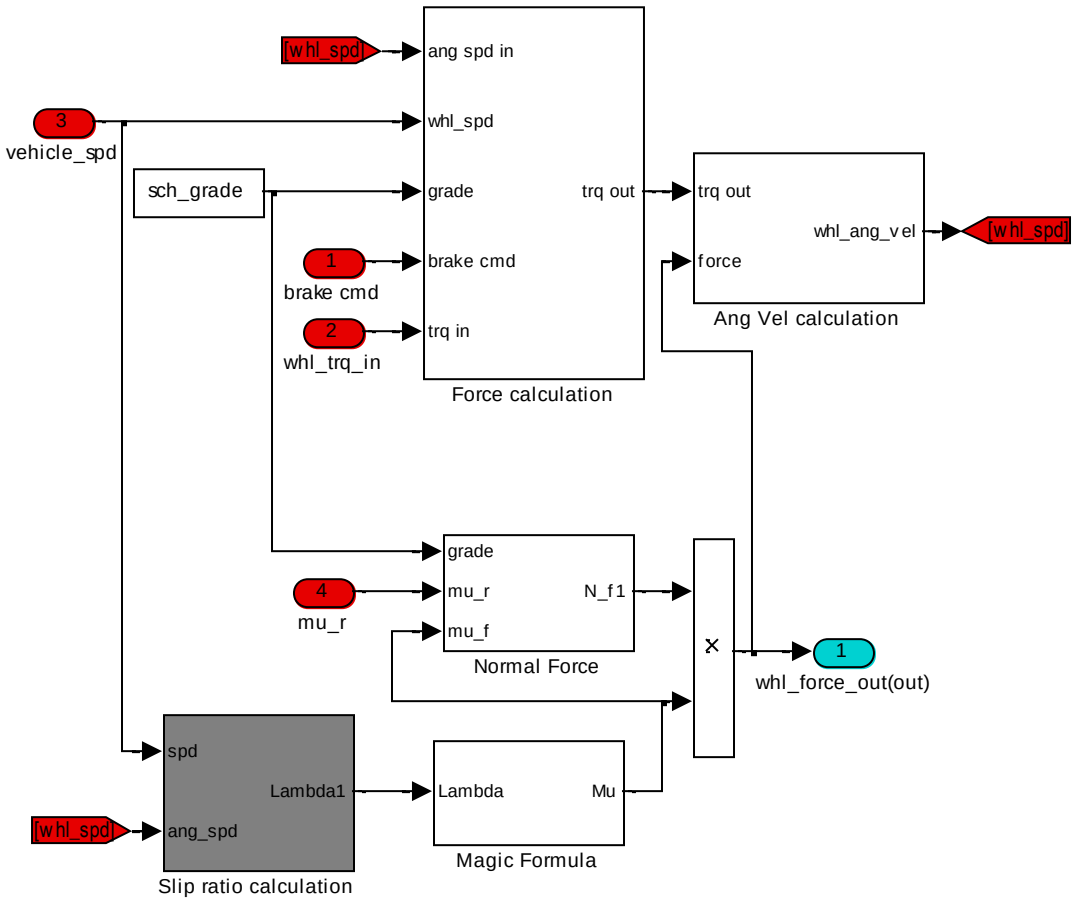

Figure 3-9 High Fidelity Wheel Model

3.2 Sensitivity Analysis of Power Management Problem

The first question that should be answered, before formulating the power management problem for IWM-EVs, is that which vehicle states have pivotal effect on the optimal solution of power management problem, and how they affect the power consumption. This investigation is called sensitivity analysis.

Minimizing the charge depletion and maximizing the driving range are the main purpose of power management system. For this, we take the change of SoC, ΔSoC as the cost function in the sensitivity analysis, and the control input as power assigned to front wheel, P_w^f. The effect of several vehicle states on the optimal P_w^f for one time step (Δt) is studies here. In Figures Figure 3-10, Figure 3-11 and Figure 3-12, the plots of ΔSoC vs P_w^f for different P_{dem}, speed and slip ratios are shown.

In Figure 3-10, we see how the optimal P_w^f changes when the speed of the vehicle changes. In low speed scenario, $v = 5\ m/s$ P_w^f has a symmetrical solution, $P_w^f = 700$ watt and $P_w^f = 4300$ watt are both the solution of the optimal power distribution problem. The same is true as of high speed scenarios, $v = 20\ m/s$ while the $P_w^f = 2000$ watt and $P_w^f = 3000$ watt are both the solutions. Differently, the optimal solution for $v = 10\ m/s$ is unique and it is half of the P_{dem} i.e $P_{w\,opt}^f = 2500$ watt.

Figure 3-11 shows the plots of P_w^f vs ΔSoC for different front wheel slip ratio, λ_f, constant speed of 10m/s and $P_{dem} = 10000$ watt. We see that, for low slip ratios, $\lambda_f = 0.01$ and $\lambda_f = 0.2$, the optimal solutions is almost symmetrical; but for high λ_f, $\lambda_f = 0.5$, the optimum P_w^f is less than half, $P_w^f = 3000$. Figure 3-12 demonstrates the optimal

solution of the problem for different P_{dem}. It is shown that, for most of the P_{dem}, the optimum solution is symmetrical except for high P_{dem} in which the ΔSoC is independent of the control input and, for all P_w^f, is the same.

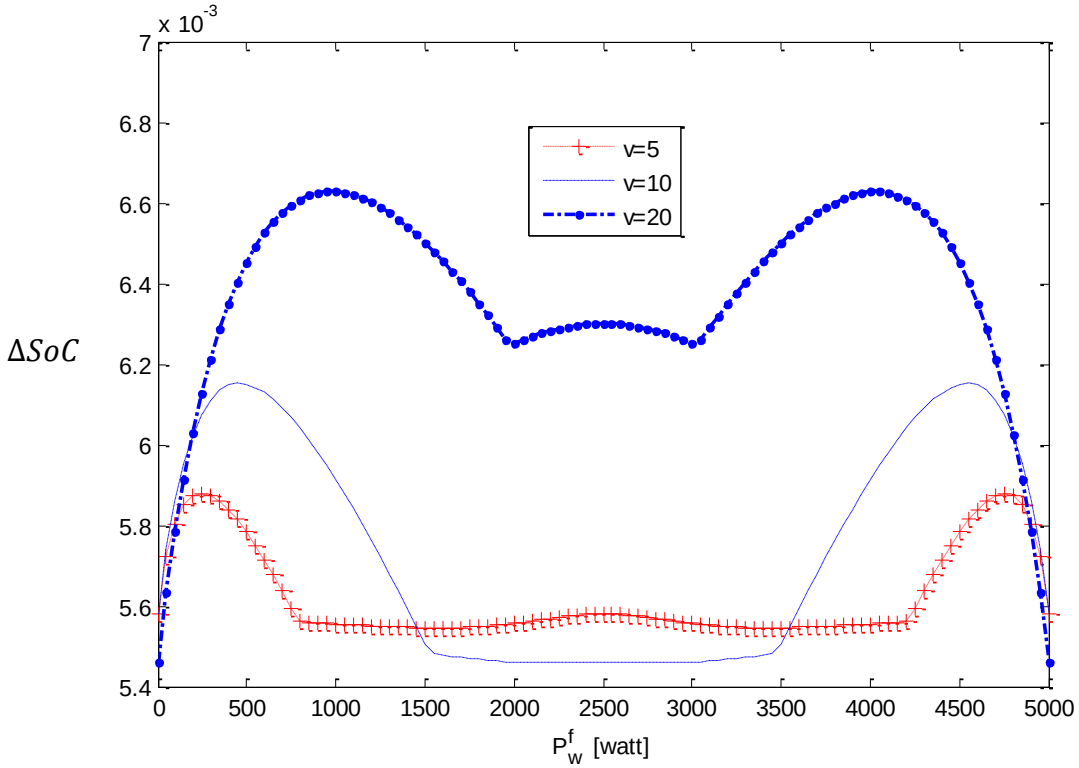

Figure 3-10 the effect of vehicle speed on ΔSoCf

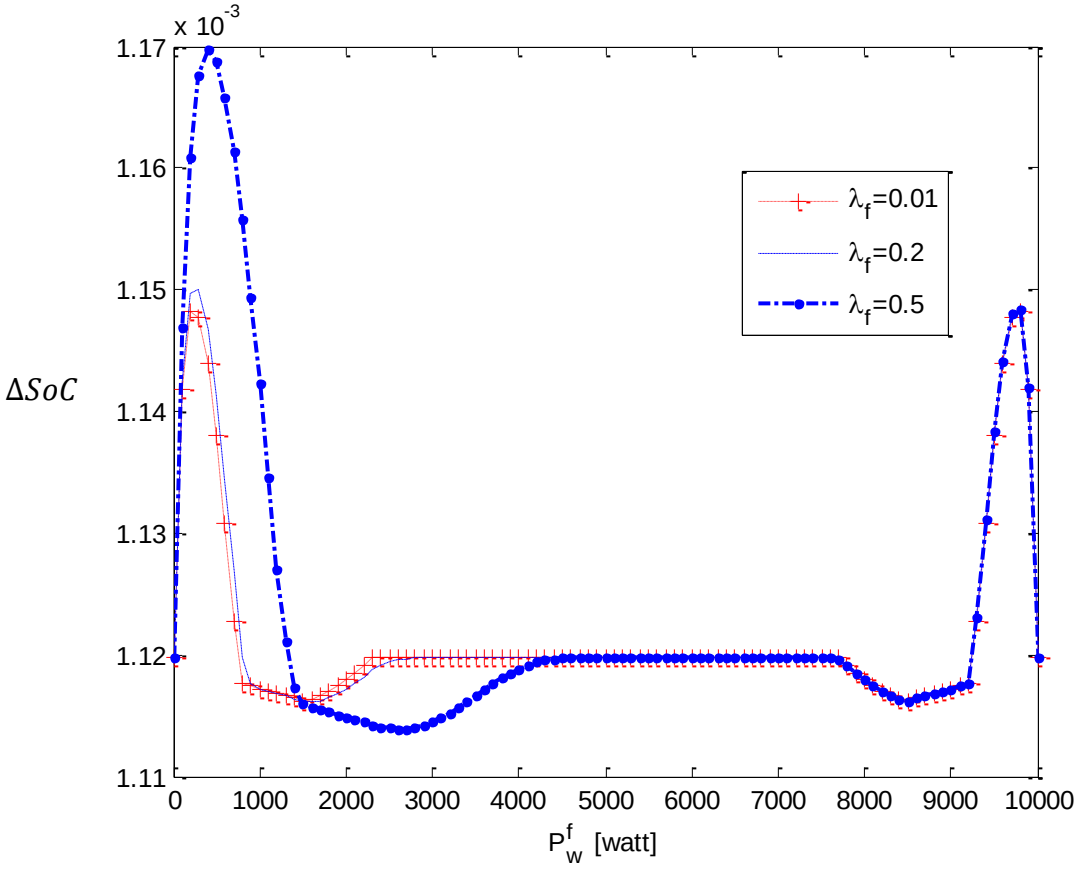

Figure 3-11 the effect of front wheel slip ratio on ΔSoC

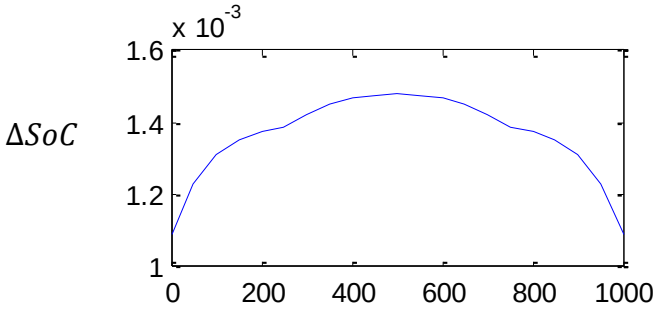

a) $P_{dem} = 1\ kw$

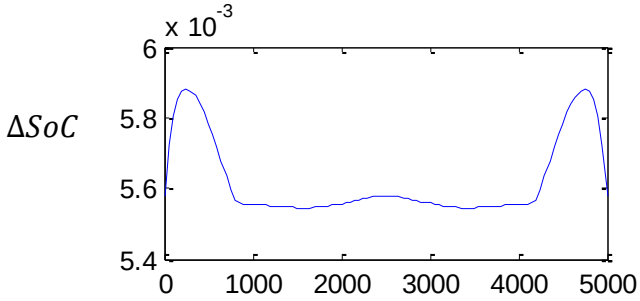

b) $P_{dem} = 5\ kw$

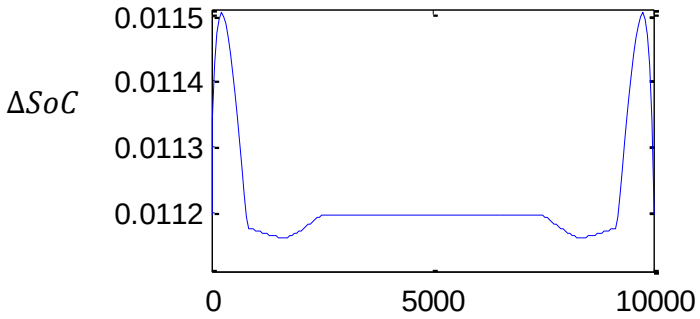

c) $P_{dem} = 10\ kw$

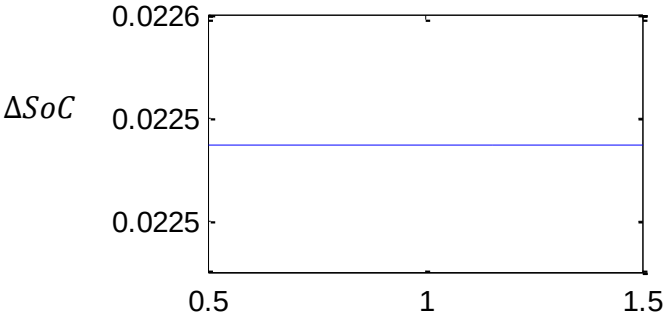

d) $P_{dem} = 20\ kw$

Figure 3-12 The effect of power distribution on the cost function (charge depletion)

3.3 Control-Oriented Model (Mathematical Model)

The control oriented model is introduced in this section. It comprises math models of chassis, wheels, in-wheel motors and battery.

3.3.1 Chassis Model

Vehicle forces and moments are shown in Figure 3-13. The vehicle longitudinal acceleration is given by:

$$a_x = \frac{1}{m}\left(F_d - F_a - F_{rr} - F_g\right) \tag{3-1}$$

where F_d is the total driving force, F_a is the aerodynamic force, F_{rr} is the roll resistance force and F_g is the gravity force that is equal to zero for flat road driving. In this thesis superscript $i = \{f1, f2, r1, r2\}$ represents wheel position in the vehicle whether front (f) or rear (r) and left (1) or right (2). For example $i = f1$ represents front left wheel. The total driving force is summation of all wheel driving forces:

$$F_d = \sum_{i=\{f1,f2,r1,r2\}} F_d^i \tag{3-2}$$

Wheel driving forces are created by the wheel-road friction and are the main external forces that move the vehicle to the desired direction. They are functions of normal force on the wheel and the friction coefficient:

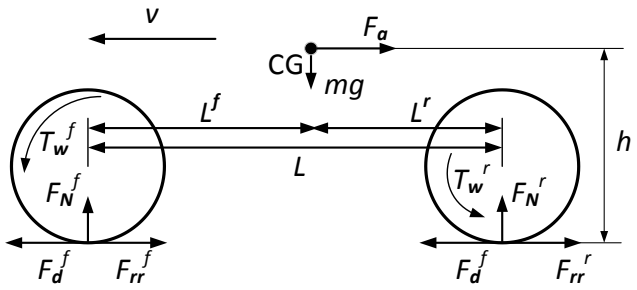

Figure 3-13 Vehicle Forces and Moments

$$F_d^i = F_N^i \mu^i \tag{3-3}$$

In the above formula, μ^i is the friction coefficient of wheel i and F_N^i is the wheel i normal force. Aerodynamic force, $F_{a,}$ is a kind of the drag force caused by movement of the vehicle in the presence of the air and calculated by:

$$F_a = \frac{1}{2}\rho A C_a v^2 \tag{3-4}$$

where ρ is the air density, A is the effective area, and C_a is aerodynamic coefficient. Equation for the roll resistance force, F_{rr} is:

$$F_{rr} = mg\ cos\ \theta\ C_{rr} \tag{3-5}$$

Where C_{rr} is roll resistance coefficient and the equation of gravitational force, F_g is:

$$F_g = mgsin\theta \tag{3-6}$$

where the angle θ is the slope of the road. The normal forces can be determined by writing the moments about the contact points for front and rear wheels. By writing and rearranging the moment equations, we have:

$$\begin{cases} F_N^{f1} = \dfrac{mg}{2L}(L^r\, cos\,\theta - h\, sin\,\theta) - \dfrac{1}{2L}(ma_x h + F_a h) \\ F_N^{r1} = \dfrac{mg}{2L}(L^f\, cos\,\theta + h\, sin\,\theta) + \dfrac{1}{2L}(ma_x h + F_a h) \end{cases} \tag{3-7}$$

As these equations show, the normal forces are functions of the total weight of the vehicle, front and rear wheelbase and the vehicle acceleration.

In the midst of SDP algorithm, we need to calculate the normal loads without having any knowledge about the vehicle acceleration, and thus by substituting equations (3-1) and (3-3) for the acceleration and driving forces, we can eliminate a_x from the normal force equations:

$$\begin{cases} F_N^{f1} = 0.5\dfrac{mgcos\theta(L^r - h\mu^r) + F_{rr}h}{L + h(\mu^f - \mu^r)} \\ F_N^{r1} = 0.5\dfrac{mgcos\theta(L^f + h\mu^f) - F_{rr}h}{L + h(\mu^f - \mu^r)} \end{cases} \tag{3-8}$$

3.3.2 Wheels Model

The well-known "Magic tire model" [45] is used to determine tire characteristics such as friction coefficient. Based on the magic formula, the wheel's friction coefficient is a nonlinear function of the slip ratio:

$$\mu_i = \mu_{max} D \sin\left(C \tan^{-1}\left(B\lambda_i - E(B\lambda_i - \tan^{-1}(B\lambda_i))\right)\right) \tag{3-9}$$

whereas μ_{max} is the maximum tire-road friction coefficient and λ_i is the slip ratio of wheel i, $i = \{f1, f2, r1, r2\}$. The meanings of the parameters B, C, D, and E can be easily found in [45]. They are assumed to be known in this study. However, μ_{max} is strongly affected by the tire–road contact conditions. For some icy roads, μ_{max} can be as low as 0.1–0.3, and thus significantly limits the braking forces. Friction coefficients vs. slip ratios for both high μ_{max} and low μ_{max} are shown in Figure 3-14; and the tire's parameters are listed in Table 3-2 that are for a typical 215/70 passenger car tire. The slip ratio is defined separately for driving and braking cases by:

Table 3-2 Tire Friction Parameters [27]

PARAMETER	VALUE
B	8.98
C	1.62
D	1
E	0.5

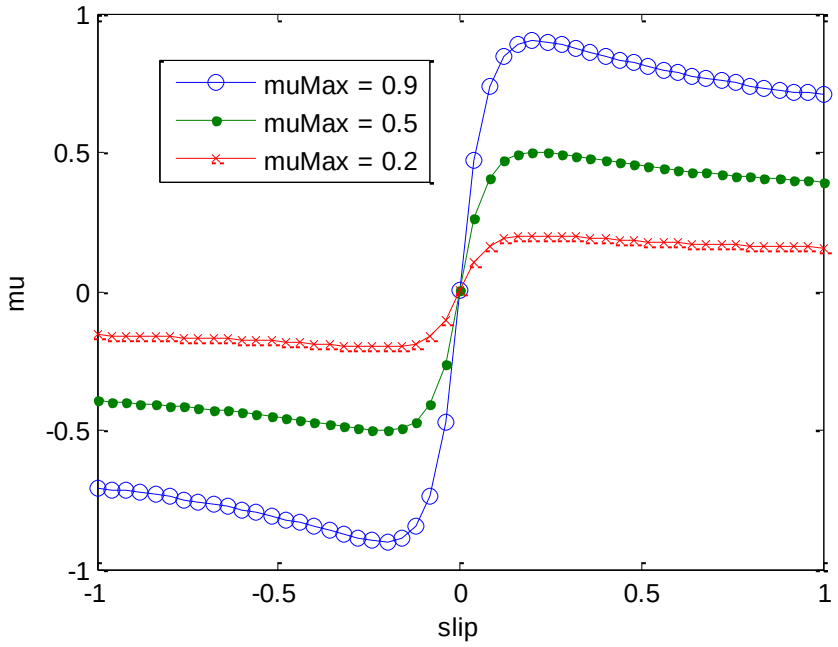

Figure 3-14 μ vs. λ calculated by the magic formula

$$\begin{cases} \lambda_i = \dfrac{r\omega_i - v}{r\omega_i} & driving \\ \lambda_i = \dfrac{r\omega_i - v}{v} & braking \end{cases} \tag{3-10}$$

whereas v is the vehicle speed and ω_i is the wheel rotational speed. External force and torque on each wheel are shown in Figure 3-13. By taking all moments about the center of front and rear wheels into consideration, equation of rotation for the wheel can be derived as:

$$\dot{\omega^{\iota}} = \frac{1}{I_W^i}\left(T_w^i - F_d^i\, r_{eff}^i\right) \tag{3-11}$$

whereas I_W^i is rotational inertia for the i-th wheel, T_w^i is the torque delivered to the wheel i and r_{eff} is effective radius of the tire. In this study, only longitudinal driving is considered; therefore, it's assumed that the left and right motors produce same torque, and the angular velocity of left and right wheels are the same:

$$\begin{aligned} T_w^{f1} &= T_w^{f2} \\ T_w^{r1} &= T_w^{r2} \\ \omega^{f1} &= \omega^{r2} \\ \omega^{r1} &= \omega^{r2} \end{aligned} \tag{3-12}$$

Therefore, one equation for the front wheel's angular velocity and one equation for rear wheel are sufficient to model the rotation of the wheels:

$$\dot{\omega}^{f1} = \frac{1}{I_W^{f1}}\left(T_w^{f1} - F_d^{f1} r_{eff}\right) \tag{3-13}$$

$$\dot{\omega}^{r1} = \frac{1}{I_W^{r1}}\left(T_w^{r1} - F_d^{r1} r_{eff}\right) \tag{3-14}$$

3.3.3 In-Wheel Motor Model

While the driver controls the vehicle's speed and acceleration by the throttle and brake pedals, in fact, he/she outlines the demanded driving power, P_{dem}, that is, the power should be excreted to the wheels to achieve the desired vehicle's velocity and acceleration. Positive P_{dem} is interpreted as the driving, and negative P_{dem} will be considered as the brake command. For every motor/generator, two power flows are defined:

1. P_{MW}: Power from (to) motors to (from) wheels.
2. P_{MB}: Power from (to) motors to (from) batteries.

In the IWM-EV, the motors are directly mounted on the wheels, and thus there is no transmission shafts, gear boxes and differentials; and consequently, there is no power lost between motors and wheels. Therefore, P_{MW} is equal to the power exerted to the wheel P_w, $P_{MW} = P_w$. To satisfy the driver's commands, the sum of all P_w should be equal to P_{dem}:

$$\sum_{i=\{f1,f2,r1,r2\}} P_w^i = P_{dem} \tag{3-15}$$

Moreover, P_{MB} equals to P_{batt}, which is the charging/discharging battery power, and $P_{MB} = P_{batt} = I_{batt}V_{batt}$; where V_{batt} and I_{batt} are the battery discharging/charging voltage and current, respectively. Because of frictional, thermal and other motor power losses, motor-battery powers P_{MB} is not the same as the motor-wheels powers P_{MW}. Therefore, motor efficiencies are defined as:

$$\eta_{trac} = \frac{P_{MW}}{P_{MB}} = \frac{P_w}{P_{batt}} \qquad for\ traction \tag{3-16}$$

$$\eta_{regen} = \frac{P_{MB}}{P_{MW}} = \frac{P_{batt}}{P_w} \qquad for\ regen\ braking \tag{3-17}$$

Each motor's efficiency is primarily a function of motor's angular velocity and torque [46]. Motor efficiency map is the key to evaluate its performance. Figure 3-7 shows efficiency maps vs. angular velocities and torques based on the experimental data from Autonomie. It can be seen from Figure 3-7 that, when the wheel speed is low, the motor efficiency drops rapidly. The efficiency map is not strictly concave or convex, which gives a merit to the power distribution strategy.

We call equation (3-15) the drivability criteria. The power management controller specifies values of the motor powers P_w^i by considering the drivability criteria as a constraint. The torques caused by these powers on the wheels are calculated by:

$$T^i = \frac{P_w^i}{\omega^i} \tag{3-18}$$

As the same as torque and angular velocity, the powers at left and right wheels are the same:

$$P_w^{f1} = P_w^{f2} = P_w^f/2$$
$$P_w^{r1} = P_w^{r2} = P_w^r/2 \tag{3-19}$$

Additionally, every motor has a maximum limit for the output power ($P_{motor,max}^{f1}$) and cannot produce power more than that value. Based on the data from Table 3-1 we have:

$$\begin{cases} P_w^{f1} \leq 7500 \\ P_w^{r1} \leq 7500 \end{cases} \tag{3-20}$$

In a braking situation, the motors work as generators and harvest kinetic energy and recharge the batteries. However, regenerative braking is limited for producing braking torque, $T_{\text{brake}}^{\text{regen}}$. Based on the data from Table 3-1, we have:

$$T_{brake}^{regen} \leq 80 \tag{3-21}$$

which means that regenerative braking cannot produce very hard brakes and friction brakes should be actuated to support regenerative brakes. Therefore, in severe braking situations where braking torque, T_{brake}, of more than 80 Nm is needed, we know that the portion of braking torque is assigned to the friction brakes, T_{brake}^{fric}.

$$T_{brake} = T_{brake}^{fric} + T_{brake}^{regen} \tag{3-22}$$

The direct consequence of this limitation is that, we cannot assume anymore that all of the braking power is harvested and charged the batteries, and we should be aware that part of barking power is lost by friction brakes, as the same as the conventional today's vehicles.

3.3.4 Battery

The battery SoC equation is derived by utilizing static equivalent circuit model, and the rate of the change of the SoC for a battery is:

$$\frac{d}{dt}(SoC) = \frac{I}{E_{max}} \tag{3-23}$$

where E_{max} is the total amount of charge that can be stored in the battery pack. The battery equivalent circuit is depicted in Figure 3-15. An internal resistor is considered for the battery model. Therefore, the battery current equation is

V

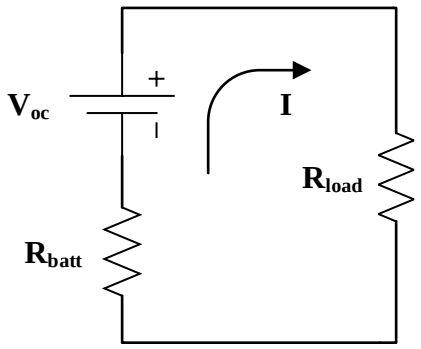

Figure 3-15 Circuit battery model

$$I = \frac{V_{oc} - V_{load}}{R_{batt}}$$

$$I^2 = \frac{IV_{oc} - P_{load}}{R_{batt}}$$

$$I^2 R_{batt} - IV_{oc} + P_{load} = 0$$

$$I = \frac{V_{oc} + \sqrt{V_{oc}^2 - 4R_{batt}P_{batt}}}{2R_{batt}}$$

In the above formula, R_{batt} is battery resistance and P_{batt} is battery power. By convention, positive P_{batt} indicates discharging and negative P_{batt} indicates charging. And thus, for SoC rate of change, we have:

$$\frac{d}{dt}(SoC) = \frac{-V_{oc} + \sqrt{{V_{oc}}^2 - 4R_{batt}P_{batt}}}{2E_{max}R_{batt}} \tag{3-24}$$

The battery power is derived from

$$P_{batt} = \sum_{i=\{f1,f2,r1,r2\}} P_w^i . \left(\eta^i\right)^{-sgn(P_w^i)} \tag{3-25}$$

where η^i is the efficiency of the i-th IWM. The battery has a maximum limit for the power output during draining and power input during recharging. While driving, if P_{dem} is higher than $P_{batt,max}$, then the battery cannot provide P_{dem}. The same is true for the regenerative braking, if high amount of power is harvested by the brakes, the battery will not save all the regenerated power. And thus, we have the following inequality for the battery power:

$$-P_{batt,max} \leq P_{batt} \leq P_{batt,max}$$

3.4 Parameter Estimation and Model Validation

To verify the modeling process of control-oriented model, the simulation results of the IWM-EV high fidelity model and control-oriented model must be compared. Small difference in these two models are acceptable because of different approaches used for modeling. To minimize the differences between high fidelity model and control-oriented model, we utilize the parameter estimation methods. Typically, in every control oriented model, there are unknown parameters that can be identified so that the simulation results of the two models become similar. This process is called parameter estimation. The high fidelity model devised in Section 3.1 is used to estimate the internal resistance of the control-oriented battery model, and to validate the accuracy in the sense that the simulation results of vehicle's control-oriented model and Autonomie high fidelity model are consistent for the same drive cycles.

Given its importance to the power management, charge depletion profile of two models should be the same, and thus the main parameter that can be manipulated is battery resistor, R_{batt}. R_{batt} is estimated based on the simulation results for urban driving cycle (Federal Test Procedure, FTP-75) and highway driving cycle (Highway Fuel Economy Test, HWFET). Root mean square error (RMSE) is used to calculate the difference between SoC of two models:

$$RMSE = \sqrt{\frac{\sum_{i=1}^{N}\left(\hat{Y}(i) - Y(i)\right)^2}{N}} \tag{3-26}$$

where $\hat{Y}$ is the SoC of the control-oriented model, Y is the SoC of the high fidelity model and N is the length of the sampling vector. The estimation is done by minimizing RMSE over R_{batt}:

$$R_{batt,est} = 0.063\ \Omega \tag{3-27}$$

Plots in Figure 3-16 compare the profiles of speed and SoC of the control-oriented and high fidelity Autonomie model for FTP75 drive cycle. Figure 3-16 shows good agreement between the two models, and therefore, it can be concluded that, control oriented model despite of its simplicity, represents the dominant dynamics of the vehicle powertrain system satisfactorily.

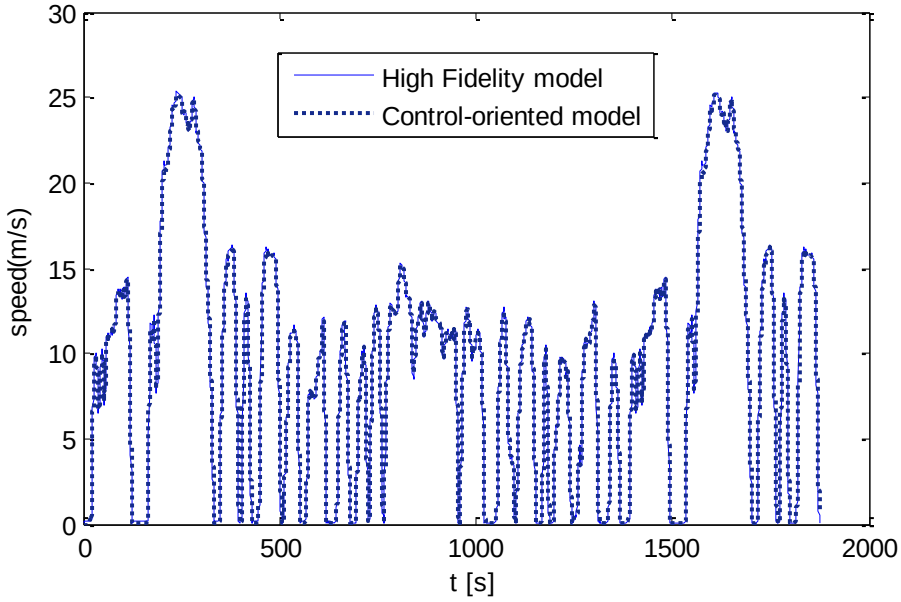

(a) Speed profiles

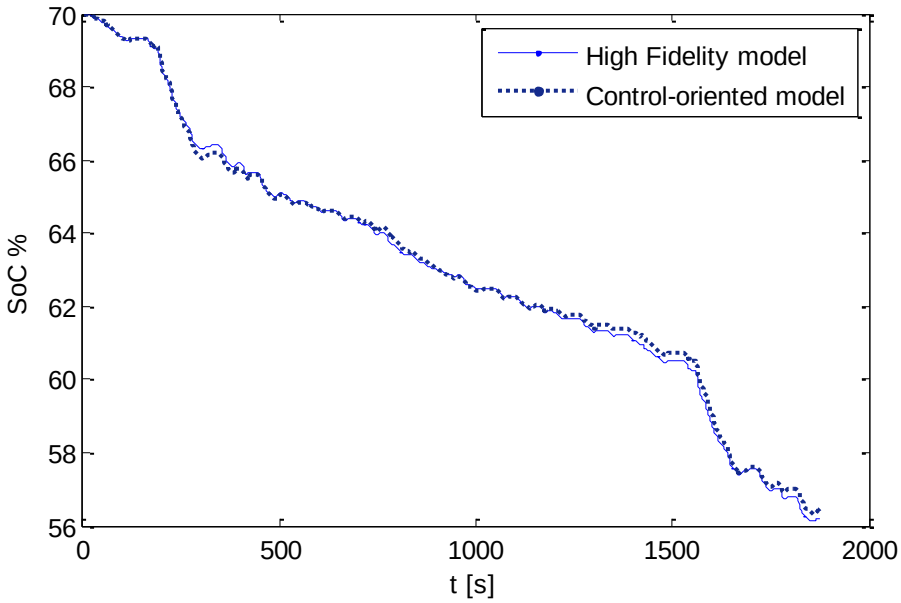

(b) SoC profiles

Figure 3-16 Comparison of speed, battery power, total torque and SoC for Autonomie and Control Oriented Model following FTP75 drive cycle

Chapter 4

Stochastic Power Management Strategy Design

In the real-world driving, there are many uncertainties for vehicle systems controllers, such as traffic flow, road speed limit, driver's desired speed, acceleration, etc. Thus, the driver's input, i.e., throttle and brake pedal commands have a stochastic and unpredictable nature. These uncertainties affect the power management problem since some power management strategies need information about the future power demand.

Offline optimal control strategies, such as Deterministic Dynamic Programming (DDP) or Pontryagin's Minimum Principle (PMP) which treat the P_{dem} as a known external input to follow a given driving cycle, are not applicable because they do not provide optimal solution to different driving cycles.

In this study, a stochastic model of driver's power demand and a SDP algorithm is utilized to solve the real-time power management problem. SDP is a computational

technique for solving stochastic, state-dependent optimization problems that find the optimum sequences of actions. Unlike DDP, the SDP control policies are time-invariant and can be used in real-time application as the same as DDP, and it can easily handle nonlinear problems with multiple constraints. A SDP model consists of five elements: decision epochs, states, actions, transition probabilities and rewards. We describe these elements in detail as follows.

4.1 Decision Epochs and Periods

The decision epochs, denoted by T, are the points of time at which the decisions are made and exerted to the plant. They consist of either a discrete set or a continuum, and either a finite or an infinite set. In discrete time problems, time is divided into periods or stages; and decisions are made at the beginning of all decision epoch. When the set of decision epochs is finite, the decision problem will be called a finite horizon problem; otherwise it will be called an infinite horizon problem.

The real-time power management problem is an infinite horizon problem since the system dynamics and the cost are time-invariant and no final time or terminal constraint is defined. A key benefit of the infinite horizon problem is that the generated control policy is time-invariant, and thus, can be easily implemented [5].

4.2 State and Action Sets

At each decision epoch, the system occupies a state, s, and the controller choose action a from the set of allowable actions in state s, denoted by A_s by observing the system and considering the states of the system. The set of possible system states is denoted by $S, s \in$

S, and the set of all possible actions is defined as A. Here, we assume that S and A do not vary with t and they are discrete and arbitrary finite sets.

Determination of the proper number of states as the controller input is an important step for the SDP, since the SDP algorithm would develop rules for all state sets and large number of states would make the problem solving slow and computationally intensive. This issue is called the curse of dimensionality. We should avoid it by trying to choose the least number of the states to capture the dominant dynamics of the system.

To find the least number of main states of the SDP problem, first, we note that for IWM-EV power management problem, despite of the HEV, the state of the charge of battery is not an important state to affect the optimal power distribution calculation. This is because the battery is the only source of power and independent of its charge level, and we should use it to provide the demanded power. Second, in section 3.2, we showed the effect of $\{P_{dem}, v, \lambda_f, \lambda_r\}$ of the optimal power management command. To obtain analytical relation between these states and optimum power distribution, we should consider that, as shown in equation (3-24), the rate of ΔSoC is function of P_{batt}. Additionally, P_{batt} changes with motor efficiencies, η^i_{trac} and η^i_{regen} and demanded power, P_{dem} as shown in equations (3-16) and (3-17). On the other hand, the motor efficiency depends on the motor rotational speed, ω, and torque, T_w; and rotational acceleration depends on the driving forces which have strong ties to the vehicle speed by equations (3-3), (3-9) and (3-10). In conclusion, it can be claimed that ΔSoC is the function of P_{dem}, vehicle speed and wheels' rotational speed. Since the slip ratio is only functions of vehicle speed and rotational speed, we substitute the rotational speeds by the slip ratio. By doing this, we make sure that the state

space will cover all of the slip ratio values which are critical for the optimal decisions. Accordingly, the states of SDP problem for this study are:

$$states: \begin{cases} P_{dem} \\ v \\ \lambda_f \\ \lambda_r \end{cases}$$

Since these states are originally continuous, we should discretize it to obtain discretized set of states. This is necessary to utilized SPD algorithm. The appropriate discretization resolution of the power demand and the time span of decision period should be simultaneously chosen such that we have an appropriate transition probability matrix of the P_{dem}. By trial and error, we found discretization sets for the problem states as below:

$$P = -12{:}\,1{:}\,19\ kW$$

$$v = \begin{bmatrix} 0 & 5 & 10 & 25 \end{bmatrix}\ m/s$$

$$\lambda_f = [\ -1\ -0.35\ -0.21\ -0.1\ \ -0.001\ \ 0\ \ 0.001\ \ 0.1\ \ \ 0.21\ \ \ 0.35\ \ 1\ ]$$

$$\lambda_r = [\ -1\ -0.35\ -0.21\ -0.1\ \ -0.001\ \ 0\ \ 0.001\ \ 0.1\ \ \ 0.21\ \ \ 0.35\ \ 1\ ]$$

$$dt_{SDP} = 0.1\ sec$$

Front in-wheel motor power P_w^f, is considered as the control input. By imposing the drivability constraint, the rear motor power P_w^r is calculated according to the power balance requirement:

$$P_f + P_r = P_{dem}$$

4.3 Decision Rules and Policies

A decision rule specifies the proper action in each state and decision epoch. Decision rules can be in the forms of Markovian or history depending on how they incorporate past information. They also may be deterministic or randomized. Our primary focus will be on deterministic Markovian decision rules.

A policy, plan, or strategy specifies the decision rule to be used at all decision epoch. It provides a prescription for action selection under any possible future system state or history. A policy π is a sequence of decision rules, $\pi = (d_1, d_2, \dots, d_{N-1})$, for a system with N decision epochs. We call a policy stationary if $d_t = d$ for all $t \in T$. A stationary policy has the form $\pi = (d, d, \dots)$; we denote it by d^{∞}.

4.4 Rewards and Costs

The system receives reward $r_t(s, a)$ at decision epoch t by choosing action a in state s whereas positive $r_t(s, a)$ may be considered as reward and income, and negative as cost. For a stationary problem with discrete state set, we have several candidates for the functions of rewards. X_t is state random variable and Y_t is action random variable.

a. The expected total reward:

$$v^{\pi} \equiv \lim_{N \to \infty} E_s^{\pi} \left\{ \sum_{t=1}^{N} r(X_t, Y_t) \right\} \tag{4-1}$$

b. The expected total discounted reward:

$$v_{\lambda}^{\pi} \equiv \lim_{N\to\infty} E_s^{\pi}\left\{\sum_{t=1}^{N} \lambda^{t-1} r(X_t, Y_t)\right\} \tag{4-2}$$

For $0 \leq \lambda < 1$

c. The average reward:

$$g^{\pi}(s) = \lim_{N\to\infty} \frac{1}{N} E_s^{\pi}\left\{\sum_{t=1}^{N} r(X_t, Y_t)\right\} \tag{4-3}$$

The proposed stochastic power management strategy in this study employs the expected total discounted reward introduced in equation (4-2). The limit in the equation (4-2) exists when $|r(s,a)| < M, \forall s \in S, \forall a \in A_s$ and $M < \infty$.

For the infinite horizon deterministic Markovian SDP problem, the expected total discounted cost is in the following form:

$$J_{\pi}(x_0) = \lim_{N\to\infty} \underset{w_k}{E}\left\{\sum_{k=0}^{N-1} \gamma^k g(x_k, \pi(x_k))\right\} \tag{4-4}$$

where $\pi(x)$ is the control policy, g is the instantaneous cost, $0 < \gamma < 1$ is the discount factor, and $J_{\pi}(x_0)$ indicates the resulting expected cost when the system starts at state x_0; and follows the policy $\pi(x)$. For the IWM-EV power management problem, the cost is a sum of the battery SoC decrease and a penalty for P_{dem} deviation; it takes the form:

$$g = \Delta SoC + \alpha . M \tag{4-5}$$

whereas α penalizes M is measured by a squared error between the demanded power and the actual power produced by wheels

$$M = \left(P_{dem} - P_f - P_r\right)^2 \tag{4-6}$$

4.5 Transition Probabilities

At every decision epoch, the system state at the next decision epoch is determined by the probability distribution $p_t(\,.\,|s\,, a)$ by choosing action a in state s. The non-negative function $p_t(j|s, a)$ denotes the probability of the system in state $j \in S$ at time $t + 1$, whereas the controller chooses action $a \in A_s$ in state s at time t. The function $p_t(j|s, a)$ is called a transition probability function.

The collection of objects $\{T, S, A_s\,, p_1(.\,|s, a), r_1(s, a)\}$ is referred as a Markov decision process. The term Markov is used since the transition probability and reward functions depend on the past only through the current state of the system and the action selected in that state.

In this study, the transition probabilities for the TPM are derived by using standard driving cycles' data. The velocity profiles of the driving cycles are considered as the observation samples and the demanded power of driving is calculated based on it. The drive cycles have been used to construct the observation samples of the stochastic system that are The Federal Test Procedure (FTP), Highway Fuel Economy Driving Schedule

(HWFET) and New York City Cycle (NYCC) as shown in Figure 4-1. Since the proposed control strategy employs demanded power TPM, we should calculate the demanded power profile from the combined driving cycle. Power demand profile of the combined driving cycles is shown in Figure 4-2. Based on the presented power demand profile, the transition probabilities is calculated and shown in Figure 4-3. One another possible approach in deriving the TPM is data logging from real-world vehicles which may consider as future work for further investigation in the power demand uncertainty problem.

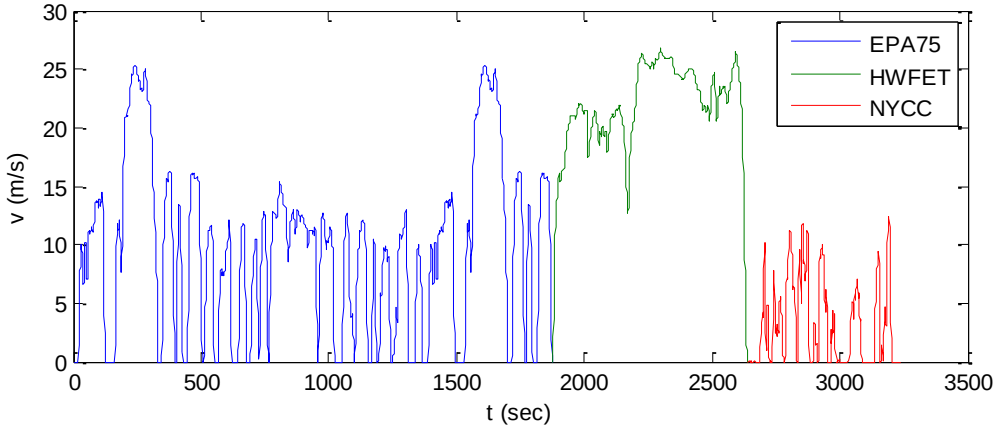

Figure 4-1 Speed Profile of the combined driving cycles

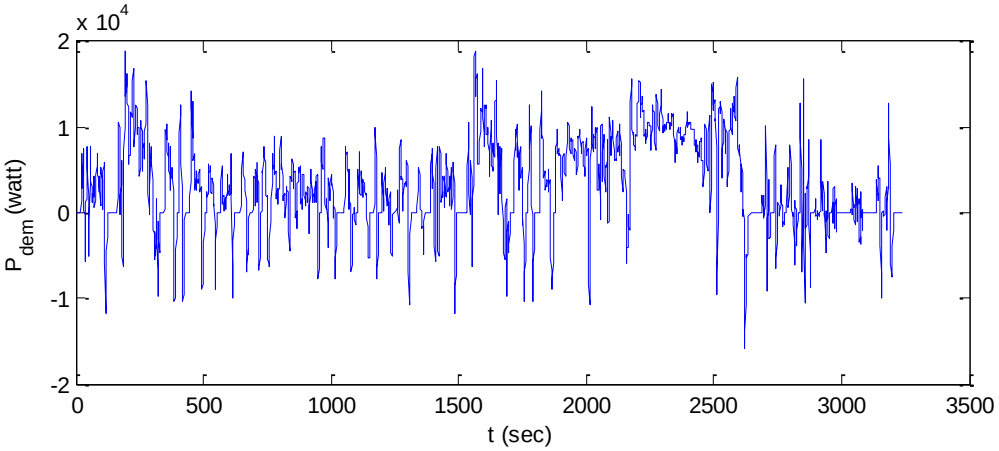

Figure 4-2 P_{dem} Profile for the combined driving cycles

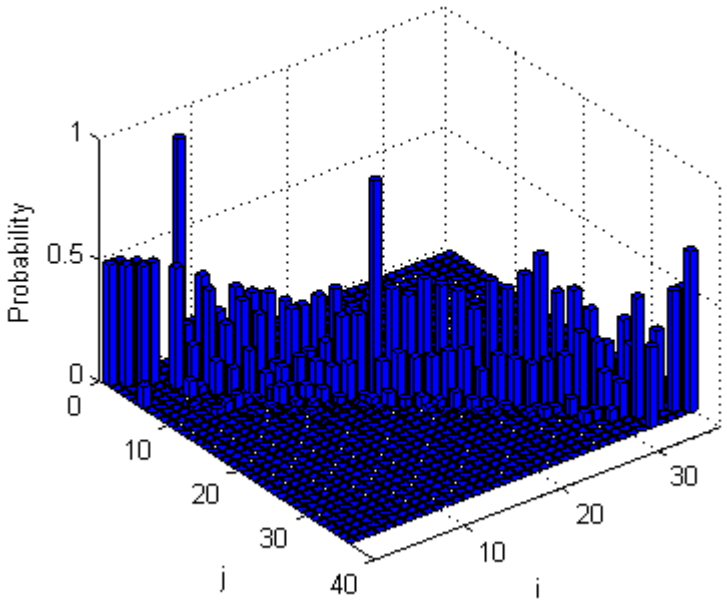

Figure 4-3 Transition Probability of power demand

To obtain the TPM from the driving cycles' data, the transition probability matrix is estimated by maximum likelihood estimation method. The demanded power P_{dem} is assumed to take finite number of values whereas N_P is the number of P_{dem} discretization:

$$P_{dem} \in \{P_{dem}^1, P_{dem}^2, \dots, P_{dem}^{N_P}\}$$

Despite of the stochastic nature of P_{dem}, it can be assumed that it has the Markov property, i.e., the probability distribution of the next step, and P_{dem} is the function of the current time step states. There probabilities are called transition probabilities:

$$Pr\{P_{dem,k+1} = P_{dem}^{j} | P_{dem,k} = P_{dem}^{i}\} = p_{i,j}$$
$$i, j = 1,2, \dots, N_P \tag{4-7}$$
$$\sum_{j=1}^{N_P} p_{i,j} = 1$$

whereas $p_{i,j}$ is one step transition probability that the system demanded power is P_{dem}^{j} at time $k+1$, and P_{dem}^{i} at time k. By assuming Markov property, power management problem can be considered as a Markov decision process to determine optimal power distribution between front and rear wheels.

The transition probability matrix is estimated on the basis of simulation results of sample drive cycles. To represent mixed city, suburban, and highway driving situations, four driving cycles are considered and P_{dem} profiles are extracted for a typical driver. The profiles of observed P_{dem} is mapped into the sequence of quantized states P_{dem}^{i} by utilizing nearest-neighbor method. Then, the transition probability is estimated by the maximum likelihood estimation method [5], which counts the observation data as:

$$\hat{p}_{i.j} = \frac{m_{i,j}}{m_i} \qquad if\ m_i \neq 0 \tag{4-8}$$

where $m_{i,j}$ is the number of occurrences of the transition from P_{dem}^{i} to P_{dem}^{j}, and $m_i = \sum_{j=1}^{n} m_{i,j}$ is the total number of the times that P_{dem}^{i} has occurred.

4.6 Stochastic Dynamic Programming Approach

There are several algorithms to solve a SDP problem. In this study, the policy iteration method, as the widely used algorithm to solve stochastic dynamic programs, is utilized to determine the optimal control policy for the control oriented model explained in section 3.3.

4.6.1 Approximate Policy Iteration Algorithm

An approximate policy iteration algorithm is used to solve the SDP problem. The IWM-EV model is used as the control oriented model which was introduced in section 3.3. The states of this model include four variables: the driver power demand, the vehicle speed, the front wheel slip ratio and the rear wheel slip ratio. The state vector $x = (P_{dem}, v, \lambda_{f1}, \lambda_{r1})$ forms a four-dimensional state space, where $v, \lambda_{f1}\ and\ \lambda_{r1}$ originally take continuous values, and P_{dem} has finite values. To solve the SDP problem, we discretize λ_{f1} and λ_{r1} as

$$\lambda_{f1} = \{{\lambda_{f1}}^1, {\lambda_{f1}}^2, \dots, {\lambda_{f1}}^{N_{Lf}}\}$$
$$\lambda_{r1} = \{{\lambda_{r1}}^1, {\lambda_{r1}}^2, \dots, {\lambda_{r1}}^{N_{Lf}}\}$$

In addition, the wheel speed is discretized:

$$v = \{v^1, v^2, \dots, v^{N_v}\}$$

The total state space is then represented by finite grids $\{x^i, i = 1,2, \dots, N_P N_v N_{Lf} N_{Lr}\}$. The control variable is $u = P_f$ which is discretized into $\{P_f^1, P_f^2, \dots, P_f^{N_u}\}$. Based on the Bellman's optimality equation, the SDP problem is solved by a policy iteration algorithm. The policy iteration algorithm consists of a policy evaluation step and a policy

improvement step in an iterative manner until the optimal policies converge to constant values, and do not change anymore. In the policy evaluation step, given a control policy π, we calculate the corresponding cost function $J_\pi(x)$ by iteratively updating the Bellman equation:

$$J_\pi^{s+1}(x^i) = g\left(x^i, \pi(x^i)\right) + \underset{\{P_{dem}^{i+1}\}}{E}\{\gamma J_\pi^s(x')\} \tag{4-9}$$

For all i, s is the iteration number, and x' is the new state, i.e.:

$$x' = f(x^i,\ \pi(x^i)) \tag{4-10}$$

which is given by the state equations (3-1), (3-13) and (3-14). However, the components of state x' do not necessarily fall exactly on the state grid. In this case, a linear interpolation of the cost function along the first two dimensions is used. In order to expedite the computations, only a fixed number of iterations are performed regardless of the convergence of the estimated cost function [38]. This method has been shown to reduce the computation time effectively [5]. In the policy improvement step, the improved policy is found through the following equation

$$\pi(x^i) = \underset{u \in U(x^i)}{argmin}\left[g(x^i, u) + \underset{\{P_{dem}^{i+1}\}}{E}\{\gamma J_\pi(\acute{x})\}\right] \tag{4-11}$$

For all i, J_π is the approximate cost function obtained from the policy evaluation step. Each of the minimizations is performed subject to the constraints. After the new policy is obtained, the algorithm comes back to the policy evaluation step to update the cost function

by using the new policy. This iterative process is repeated, until J_π converges within a selected tolerance level. This algorithm‘s flowchart is depicted in Figure 4-5.

The discount factor is $\gamma = 0.8$ and the weighting factor α is chosen as 10^{-4}. The policy iteration procedure is terminated when the policy of two successive iterations is equal. The Figure 4-4 shows the convergence fashion of the policies of the SDP. To plot Figure 4-4, we calculated the norm of policy vector in each iteration of the SDP algorithm, and the change of the norm of the policy vector in each iteration is plotted. We can see that, after 5 iterations, the algorithm converged. The resulting policy is in the form of a look-up table, $P_f(P_{dem}, v, \lambda_f, \lambda_r)$, i.e., the optimal front power P_f is a function (look-up table) of total demanded power, vehicle speed, and front and rear slip ratios. The desired rear motor power can then be calculated from $P_r = P_{dem} - P_f$.

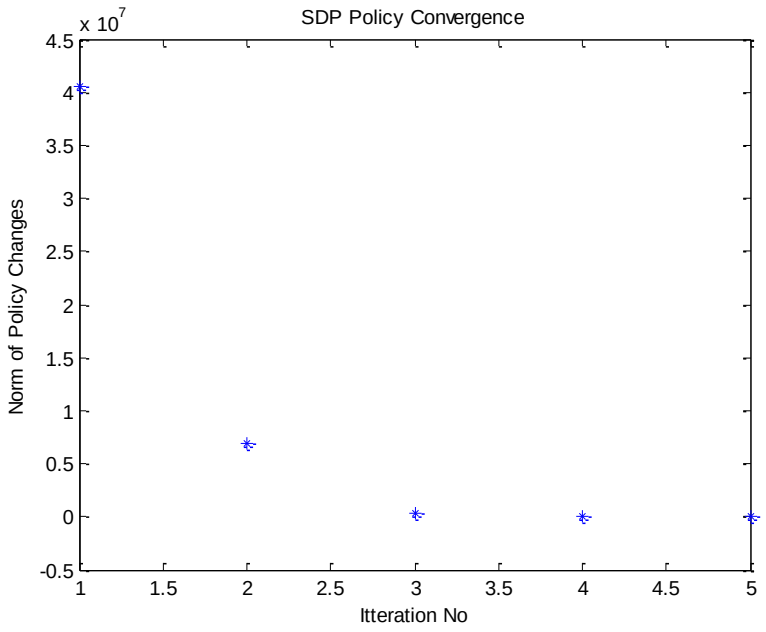

Figure 4-4 Policy iteration convergence

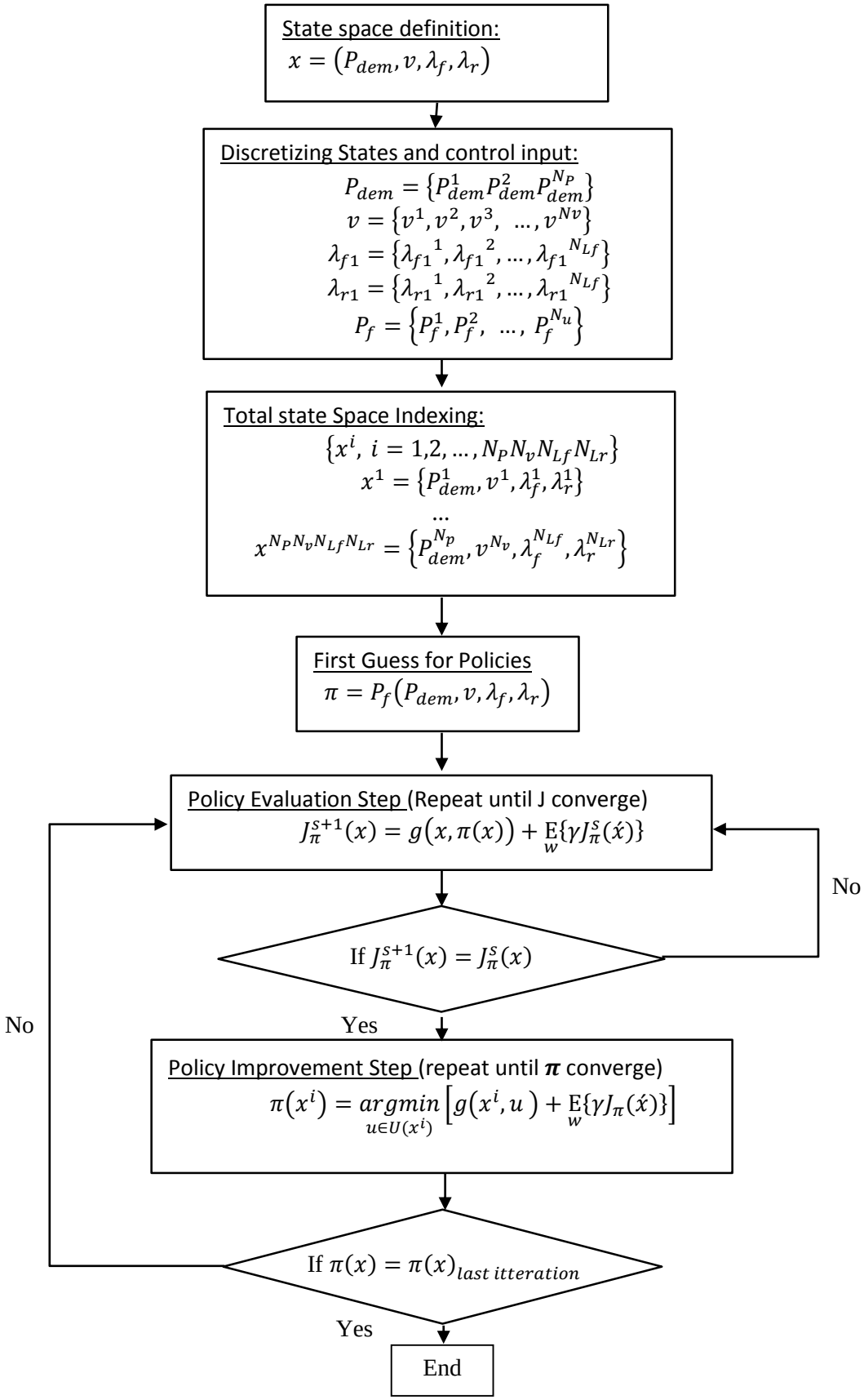

Figure 4-5 The approximate policy iteration algorithm flowchart

4.6.2 Constraints

There are several constraints for this problem. First of all, the optimization is subject to equality constraints as the system equations described in Section Chapter 3. The first constraint is the driving torque limit of electric motors:

$$T_i \leq T_{max\,motor} \quad (for\ Driving) \tag{4-12}$$

The next constraint is the limitation of regenerative breaking. During breaking, if the demanded break exceeds the limit, the breaking is divided to regenerative and frictional breaking

$$\begin{gathered} T_i = T_{regen} + T_{friction}: \\ T_{regen} \leq T_{max\,regen} \quad (for\ Breaking) \end{gathered} \tag{4-13}$$

The last constraint is the limitation of battery to deliver power:

$$P_{batt,min} \leq P_{batt} \leq P_{batt,max} \tag{4-14}$$

4.6.3 Benchmarks

To compare the performance of SDP control scheme, two benchmark power management strategies are considered. The first is the equal distribution scheme which is a sort of the fixed ratio distribution. Fixed ratio distribution strategies, regardless of the states of the vehicle, assign the driving powers as the constant gain of the total demanded powers:

$$P_w^f = \gamma P_{dem}$$
$$P_w^r = (1-\gamma) P_{dem} \tag{4-15}$$

whereas γ is the distribution ratio and it is between zero and one. The optimal γ is investigated in this study numerically, and as the result, $\gamma = 0.5$ is the globally optimal distribution ratio. Therefore, equal distribution is the optimal solution of the fixed ratio distribution strategy.

The second power management strategy, as the benchmark, is the generalized DP rule-base system. Since the dynamic programming solution is drive cycle dependent, the rules from one drive cycle may cause bad results for another drive cycle, thus the generalized rule based system from Ref [47] is proposed. To determine the generalized DP rule-based system, first, we solved the dynamic programming for specific drive cycle, FTP75, and then calculated a simple linear relation between P_{dem} and P_w^f. The solution of dynamic programming for FTP driving cycle and a single rule extracted from P_f vs P_{dem} profile is shown in Figure 4-6.

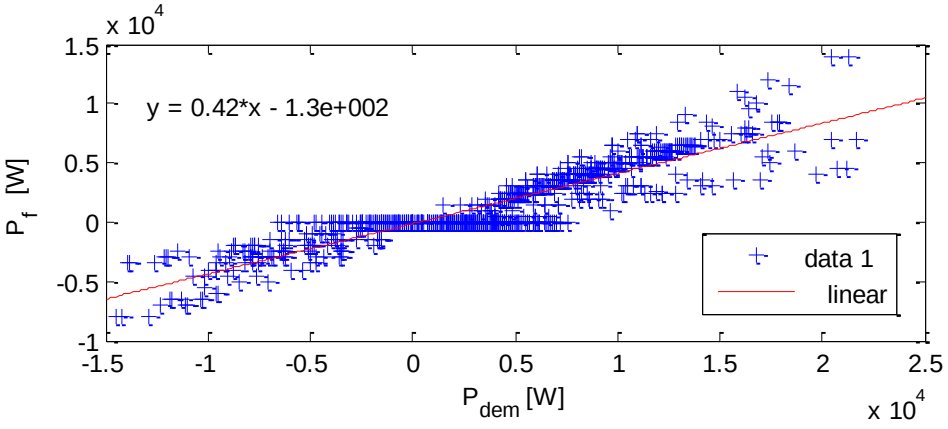

Figure 4-6 Dynamic programming optimal P_f vs total P_{dem}

4.7 Skid Avoidance System Integration to Power Management Strategy

To prevent safety issues while using the power management strategy, a skid avoidance and anti-lock brake system, ABS, is implemented as part of the power management system of the IWM-EV. In the conventional vehicle ABS system, a high frequency bang–bang controller as an on–off controller, is used to keep the slip ratios in the desired interval to maximize the braking performance. Since the electric motor's response time is much faster than typical ABS of ICE vehicles [9], the task of ABS can be easily handled by electric motor power controller.

In this study, a set of skid avoidance constraints are proposed to be considered in development of the stochastic dynamic programing policies. The proposed constraints for the slips are presented in Table 4-1. The main logic behind proposing these constrains is that, in each IWM, while performing hard brakes if the wheel's slip ratio violates the desired interval, the power management controller should set the brake command to zero to relax the braking system and avoid the violation.

Due to the baseline vehicle wheel specifications, as it can be seen in Figure 3-4, the critical slip ratios is equal to ± 0.2, and thus the desired slip ratio interval is:

$$\lambda = [-0.2, +0.2]$$

Therefore, we proposed in constraints of Table 4-1 that when $\lambda_f < -0.2$, the front IWM commanded power, P_f, should be zero; and the same is for the rear IWM. Consequently,

the only situation in which the power distribution problem is over-actuated and has two degree of freedom is the case that both wheels' slip ratio are inside the desired interval.

Table 4-1 Skid Avoidance Constraints

	$\boldsymbol{\lambda_f < -0.2}$		$\boldsymbol{\lambda_f \geq -0.2}$	
$\boldsymbol{\lambda_r < -0.2}$	$P_f = 0$	$P_r = 0$	$P_f = P_{dem}$	$P_r = 0$
$\boldsymbol{\lambda_r \geq -0.2}$	$P_f = 0$	$P_r = P_{dem}$	Search for the best distribution	

The simulation results of implementing the integrated skid avoidance and stochastic power management strategy are presented in section 5.2.

Chapter 5

Power Management Strategy Evaluation

In this chapter, the results of utilizing the proposed stochastic power management strategy are presented and its performance is compared with the other power distribution schemes. For this investigation, we developed the high fidelity IWM-EV model which is introduced in section 3.1. The evaluations show that the stochastic power management strategy saves up to 22% in power consumption while following the desired drive cycles seamlessly. As follows, the integrated power management and skid avoidance system is evaluated in section 5.2. We are benefited from the perfect potential of the SDP to handle nonlinear problems and constraints by defining constraints for slip ratios to maintain them in the desired intervals.

5.1 Stochastic Power Management Strategy

The output of the policy iteration algorithm introduced in section 4.6 is a set of rules specifying the front and rear wheels powers based on the current states of the vehicle. After obtaining these rules, we need to evaluate the optimality of the strategy by comparing it with the other strategies. The most important index for comparing the power management strategies is the change of the state of the charge during driving $as\ \Delta SoC = SoC_i - SoC_f$. Smaller ΔSoC is desired for us since it means that less power is consumed, the power management strategy is more efficient, and the electric vehicle's range is larger.

To evaluate the stochastic power management strategy, we simulated the high fidelity vehicle model which employed the stochastic power management system for four different drive cycles, as FTP, HWFET, NYCC and USSD. The first three drive cycles of FTP, HWFET and NYCC have been used for the observation process of the TPM calculation in section 4.4. In addition to these drive cycles, the performance of the stochastic power management strategy for USSD drive cycle is presented to investigate the robustness and generality of the obtained power management scheme. We performed the drive cycle simulations for two other power management strategies, equal distribution and generalized DP rule-based system introduced in section 4.2 as the benchmarks for the comparison.

Table 5-1, Table 5-2 and Table 5-3 show the comparison of ΔSoC for the three control schemes for the FTP, HWFET, NYCC and USSD drive cycles for different road conditions. The maximum friction coefficient of the results of Table 5-1 is $\mu_{max} = 0.9$ which typically belongs to asphalt road driving while μ_{max} for Table 5-2 and Table 5-3 are 0.5 and 0.2 respectively.

By Comparison of these tables, it concludes that, for all road conditions, SDP is better than equal distribution and generalized DP rule-based up to 22%. The improvement of the SDP than the equal distribution increases as the μ_{max} decreases, which means that in slippery road condition, SDP strategy performs much better than the equal distribution and generalized DP rule-based strategies. The simulation results show that the performance of the equal distribution and generalized DP rule based system is almost the same. Interestingly, the linear relation for the generalized DP rule-based system is similar to equal distribution since it is $P_w^f = 0.42 * P_{dem} + 1300$.

The performance of the stochastic power management strategy for the USSD drive cycle is as good as for the other drive cycles in Table 5-1, Table 5-2 and Table 5-3. Therefore, we can claim that the stochastic drive cycle is a robust power management strategy for all drive cycles and real time applications.

The powers assigned to the front and rear wheels, P_f and P_r, versus time for USSD drive cycle in a snowy road with $\mu_{max} = 0.2$ as shown in Figure 5-1. Due to these plots, we can see that the severe brake demands are assigned to the front wheels. And thus, in several instances, the front wheels starts locking and slip ratios goes to -1, besides, the power consumption is reduced and final state of the charge is increased.

Table 5-1 ΔSoC for High-fidelity Model Simulation ($\mu_{max} = 0.9$)

Drive Cycle	Fixed Ratio	DP Rules	SDP	% saved
FTP	13.8	13.79	13.71	0.65
HWFET	14.88	14.86	14.68	1.34
NYCC	1.585	1.58	1.58	0.32
USSD	8.78	8.77	8.72	0.68

Table 5-2 ΔSoC for High-fidelity Model Simulation ($\mu_{max} = 0.5$)

Drive Cycle	Fixed Ratio	DP Rules	SDP	% saved
FTP	13.89	13.87	13.6	2.09
HWFET	14.92	14.90	14.73	1.27
NYCC	1.6	1.59	1.53	4.37
USSD	8.84	8.82	8.67	1.92

Table 5-3 ΔSoC for High-fidelity Model Simulation ($\mu_{max} = 0.2$)

Drive Cycle	Fixed Ratio	DP Rules	SDP	% saved
FTP	14.3	14.29	14.19	0.77
HWFET	15.04	15.01	14.93	0.73
NYCC	3.41	3.4	2.64	22.58
USSD	9.09	9.09	9.07	0.22

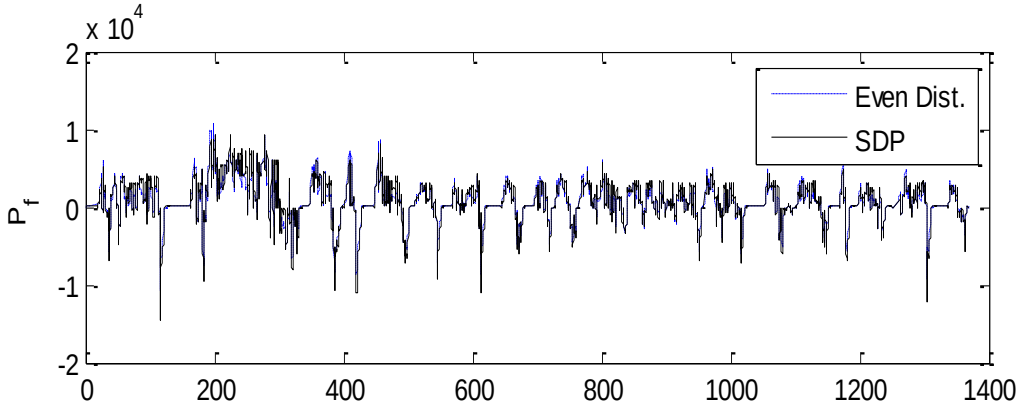

(a)

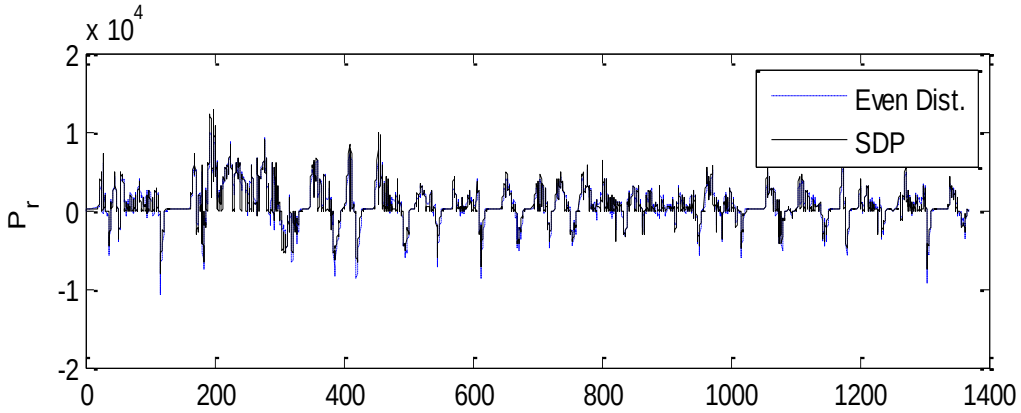

(b)

Figure 5-1 Commanded power comparison between SDP and equal power distribution for low friction condition $\mu_{max} = 0.2$ (a) front IWM (b) rear IWM

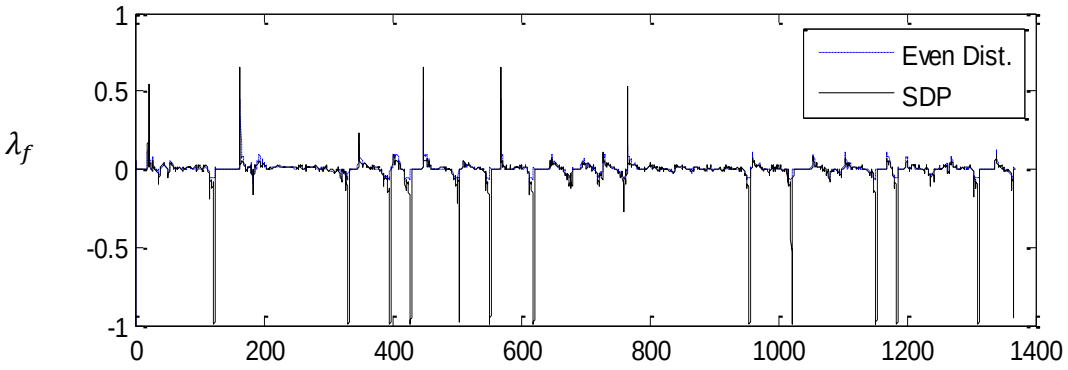

(a)

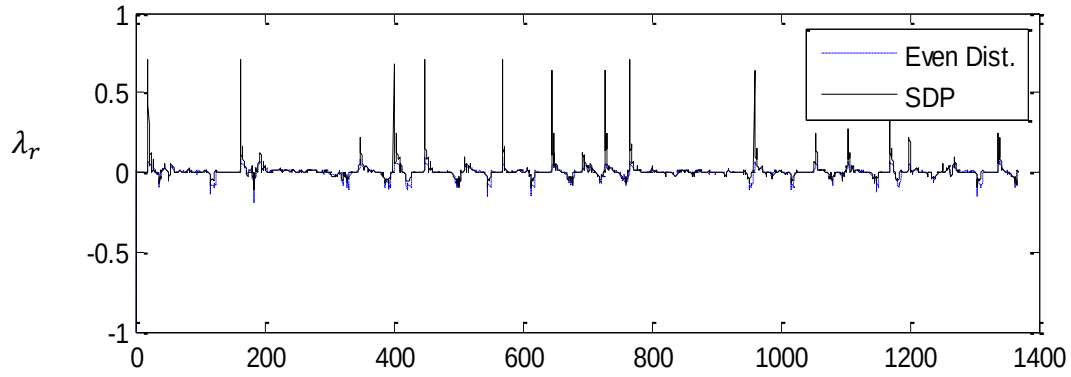

(b)

Figure 5-2 Slip ratio comparison between SDP and equal power distribution for low friction condition $\mu_{max} = 0.2$ (a) front IWM (b) rear IWM

5.2 Integrated Skid Avoidance and Power Management System

In Figure 5-2, the slip ratios of a driving simulation at the slippery road condition are depicted. We can see that, in many braking instances, the slip ratio of the front wheel converges to -1 which means full locking of the wheel. Wheel lockage is a highly undesirable event during the driving since it causes braking ineffectiveness and loss of the steering controllability.

In section 4.7, the proposed integrated power management and skid avoidance system was introduced. This control strategy optimizes the power consumption and keeps the wheels' slip ratios in the desired intervals simultaneously. The simulation results of utilizing this control scheme as the power distribution system is in this section. The result of this section shows us that adding skid avoidance constraints to the power management prevents the wheels from locking in the severe barking while maintains the optimality of the power management strategy.

Figure 5-3 and Figure 5-4 show the slip ratios and torque profiles of the front and rear wheels for SDP strategy, integrated skid avoidance and power management strategy. From Figure 5-3, we can see that the integrated strategy has done its task flawlessly and has maintained the braking slip rations in the acceptable interval. In fact, the proposed integrated control scheme prevents the wheel motors to produce high torques when the slip ratio violated from the limits. These results show that the presence of these constraints makes the power management controller brake in a more effective manner. Based on the charge depletion comparison of Table 5-4, the skid avoidance integrated strategy is similar to SDP strategy, which means that adding the skid avoidance constraints to the stochastic power management strategy did not change the power depletion of the vehicles at all. In

conclusion, we can say that, integrated skid avoidance and stochastic power management strategy improves the braking performance and decreases the power consumption in comparison to strategies such as equal distribution and generalized DP rule-based.

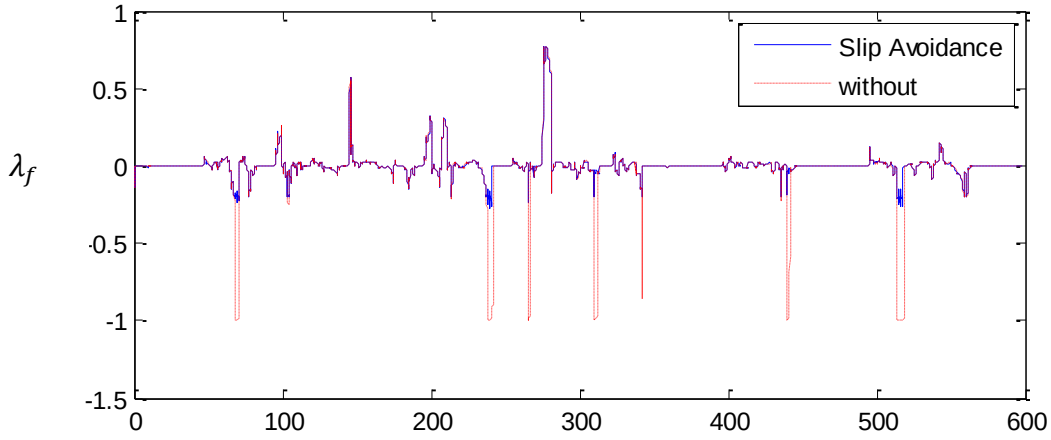

(a)

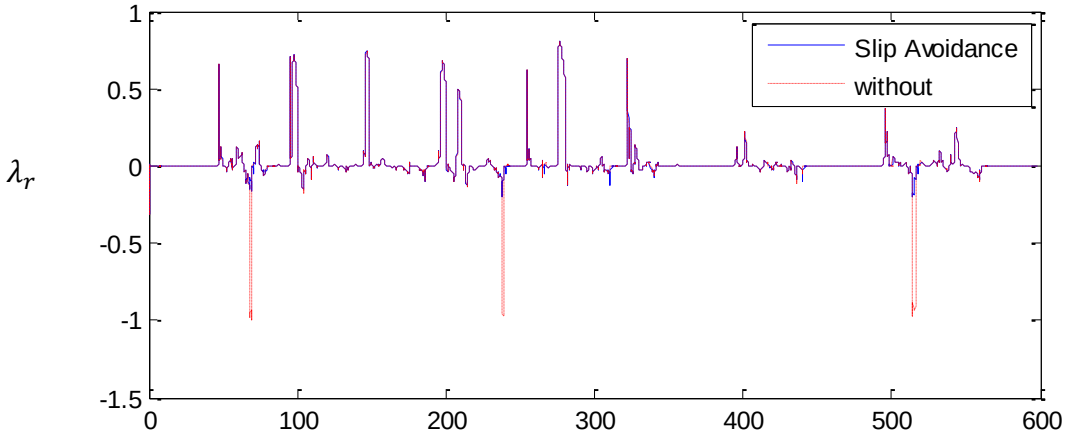

(b)

Figure 5-3 Slip ratio comparison for power management system with skip avoidance and without skip avoidance constraint for (a) front and (b) rear wheels

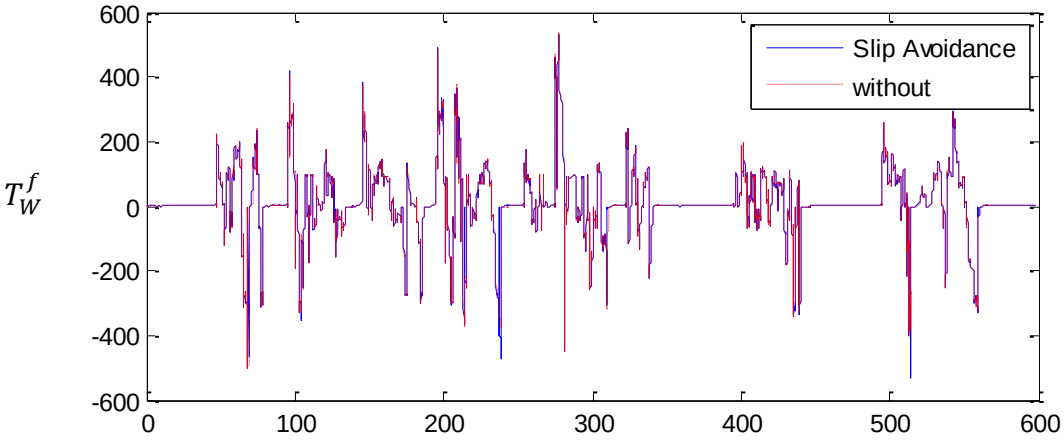

(a)

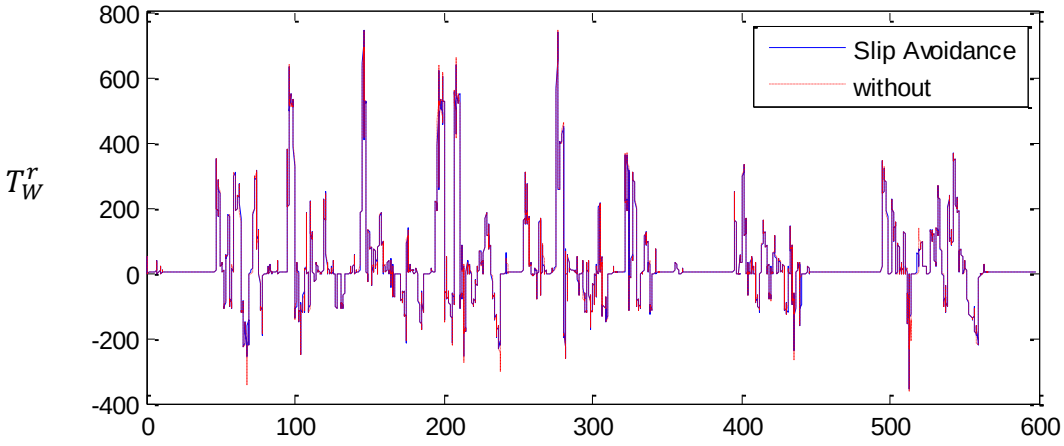

(b)

Figure 5-4 commanded torques comparison for power management system with skip avoidance and without skip avoidance constraint for (a) front and (b) rear wheels

Table 5-4 ΔSoC for High-fidelity Model Simulation ($\mu_{max} = 0.2$)

Drive Cycle	SDP	SDP with skid avoidance
FTP	14.19	14.19
HWFET	14.93	14.93
NYCC	2.64	2.64
USSD	9.07	9.07

Chapter 6

Conclusions and Future Works

In the first section of this chapter, the conclusions of implementing the proposed strategy are discussed. In the second section, the future works are listed.

6.1 Conclusions

In this thesis, a novel power management strategy for IWM-EVs is developed. The proposed power management strategy utilizes SDP to take into the account the stochastic nature of the driving commands of the driver. And then, a skid avoidance algorithm is integrated to the power management strategy to keep the wheels' slip ratio in the desired interval.

To apply SDP, it is assumed that the demanded power by the driver is a Markov process, and then, several driving cycles are considered to generate acceptable probability distributions for the demanded power. The selected drive cycles were used for the evaluation of the proposed strategy. Four states are considered as the stochastic power management inputs: the demanded power, the vehicle's speed, and the front and the rear

wheels' slip ratios. A high fidelity vehicle model and a control-oriented vehicle model are developed in this study. The high fidelity modeling is accomplished in the Simulink environment for the purpose of power management strategy evaluation, control-oriented model verification and sensitivity analysis; and control oriented model is developed for parameter optimization of the algorithm. The parameter optimization of the proposed strategy is done for a baseline vehicle.

The evaluation of the proposed power management strategy for different driving cycles and road conditions shows that it decreases the charge depletion while providing the demanded power for the IWMs without any problem. As the result, the vehicle employing this power management strategy can track the driving cycles perfectly and has more final SoC in comparison to the equal distribution strategy and DP extracted rule-base strategy. The obtained stochastic power management strategy saves up to 22% SoC in comparison to equal distribution power management strategy.

Despite of the intelligent vehicle systems, which employ extra sensors and communicating systems to determine future speed profile of the vehicles, SDP is free to lunch and only handles past driving information to predict the future situation.

Skid avoidance algorithm consists of several constraints which limit the power management strategy output based on the wheels' slip ratios. The response time of the IWMs is much faster than a typical ABS, and thus the anti-brake and skid avoidance algorithms can be easily handled by motors' power control. The simulation results of integration of the power management strategy and skid avoidance systems show that integrated skid avoidance and stochastic power management strategy improve the braking

performance and decrease power consumption in comparison to strategies such as equal distribution or generalized DP rule-based.

Up to the author's knowledge, this thesis contains these contributions:

- This study is the first utilization of the SDP for the IWM-EVs.
- It is the first time that the slip ratios are considered as the decision variables of the SDP power management problem.
- Skid avoidance integration with power management strategy is for IWM-EVs.

6.2 Future Works

Based on the problems explained and studies in this thesis, there are several research opportunities in IWM modeling, stochastic power management and skid avoidance algorithms can be considered for continuation of this research:

- Data gathering from real experiments can be done to have a more reliable probability distributions and matrix of TMP.
- Other algorithms of SDP of reference [5] can be utilized to compare the optimality of solutions and find the best SDP for this problem.
- Better and more sophisticated skid avoidance algorithm can be implemented.
- Utilizing hardware-in-the-loop, HIL, methods can be used to validate the proposed strategies.

REFERENCES

[1] Electric Drive Transportation Association, “Electric Drive Sales Dashboard,” 2014. [Online]. Available: http://electricdrive.org/index.php?ht=d/sp/i/20952/pid/20952. [Accessed: 26-Feb-2014].

[2] T. Trigg and P. Telleen, “Global EV Outlook,” 2013.

[3] I. Husain, *Electric and hybrid vehicles: design fundamentals*. CRC PRESS, 2003.

[4] PROTEAN ELECTRIC, “Protean Drive PD18 Subsystems.” [Online]. Available: http://www.proteanelectric.com/en/subsystems/. [Accessed: 07-May-2014].

[5] M. L. Puterman, *Markov Decision Processes: Discrete Stochastic Dynamic Programming*. John Wiley & Sons, 2009, p. 672.

[6] A. Watts, A. Vallance, A. Fraser, A. Whitehead, C. Hilton, H. Monkhouse, J. Barrie-Smith, S. George, and M. Ellims, “Integrating In-Wheel Motors into Vehicles - Real-World Experiences,” *SAE Int. J. Alt. Power*, vol. 1, no. 1, pp. 289–307, Apr. 2012.

[7] Y. Hori, “Future vehicle driven by electricity and control-research on four-wheel-motored‘ UOT Electric March II,’” *IEEE Trans. Ind. Electron.*, vol. 51, no. 5, pp. 1–14, 2004.

[8] Tetsuya Suzuki, K. Shimamura, and Y. Maeda, “Development of Electric Commuter Concept Car ‘C-ta,’” *SAE*, 2011.

[9] H. Fujimoto, “Regenerative brake and slip angle control of electric vehicle with in-wheel motor and active front steering,” in *Proceedings 1st International Electric Vehicle Technology Conference*, 2011.

[10] Z. Yan-e, Z. Jianwu, and H. Xu, “Development of a High Performance Electric Vehicle with Four-Independent-Wheel Drives,” in *SAE International Powertrains, Fuels and Lubricants Congress*, 2008.

[11] B. Jacobsen, “Potential of electric wheel motors as new chassis actuators for vehicle manoeuvring,” *Proc. Inst. Mech. Eng. Part D J. Automob. Eng.*, vol. 216, no. 8, pp. 631–640, Aug. 2002.

[12] P. He, Y. Hori, M. Kamachi, K. Walters, and H. Yoshida, “Future motion control to be realized by in-wheel motored electric vehicle,” in *31st Annual Conference of IEEE Industrial Electronics Society*, pp. 6–10, 2005.

[13] L. Jin, C. Song, and Q. Wang, “Influence of In-Wheel Motor Structure about the Contact and Comfort for Electric Vehicle,” *2010 2nd Int. Work. Intell. Syst. Appl.*, pp. 1–5, May 2010.

[14] L. De Novellis, A. Sorniotti, and P. Gruber, “Optimal Wheel Torque Distribution for a Four-Wheel-Drive Fully Electric Vehicle,” *SAE Int. J. Passeng. Cars - Mech. Syst.*, vol. 6, no. 1, pp. 128–136, Apr. 2013.

[15] K. Jalali, T. Uchida, S. Lambert, and J. McPhee, “Development of an Advanced Torque Vectoring Control System for an Electric Vehicle with In-Wheel Motors using Soft Computing Techniques,” *SAE Int. J. Altern. Powertrains*, vol. 2, no. 2, pp. 261–278, Apr. 2013.

[16] L. Jin, C. Song, and C. Hu, “Driving force power steering for the electric vehicles with motorized wheels,” *2009 IEEE Veh. Power Propuls. Conf.*, pp. 1518–1524, Sep. 2009.

[17] C. Geng, T. Uchida, and Y. Hori, “Body slip angle estimation and control for electric vehicle with in-wheel motors,” in *Industrial Electronics Society, 2007*, 2007, no. 1, pp. 351–355.

[18] W. Kim and K. Yi, “Coordinated Control of Tractive and Braking Forces Using High Slip for Improved Turning Performance of an Electric Vehicle Equipped with In-Wheel Motors,” *2012 IEEE 75th Veh. Technol. Conf. (VTC Spring)*, pp. 1–5, May 2012.

[19] S. Sakai, S. Member, H. Sado, and Y. Hori, “Motion Control in an Electric Vehicle with Four Independently Driven In-Wheel Motors,” vol. 4, no. 1, pp. 9–16, 1999.

[20] C. Chang, “Torque distribution control for electric vehicle based on traction force observer,” *2011 IEEE Int. Conf. Comput. Sci. Autom. Eng.*, no. 3, pp. 371–375, Jun. 2011.

[21] H. Liu, X. Chen, and X. Wang, “Overview and Prospects on Distributed Drive Electric Vehicles and Its Energy Saving Strategy,” no. 7, pp. 122–125, 2012.

[22] W. Xu, H. Zheng, and Z. Liu, “The Regenerative Braking Control Strategy of Four-Wheel-Drive Electric Vehicle Based on Power Generation Efficiency of Motors,” Apr. 2013.

[23] J. Gu, M. Ouyang, D. Lu, J. Li, and L. Lu, “Energy efficiency optimization of electric vehicle driven by in-wheel motors,” *Int. J. Automot. Technol.*, vol. 14, no. 5, pp. 763–772, 2013.

[24] H. Qian, G. Xu, J. Yan, T. L. Lam, Y. Xu, and K. Xu, “Energy management for four-wheel independent driving vehicle,” *2010 IEEE/RSJ Int. Conf. Intell. Robot. Syst.*, pp. 5532–5537, Oct. 2010.

[25] Y. Chen, Z. Chen, and J. Wang, “Operational Energy Optimization for Pure Electric Ground Vehicles Based on Terrain Profile Preview,” *ASME 2011 Dyn. Syst. Control Conf. Bath/ASME Symp. Fluid Power Motion Control. Vol. 2*, pp. 271–278, 2011.

[26] K. Maeda, H. Fujimoto, and Y. Hori, “Four-wheel driving-force distribution method based on driving stiffness and slip ratio estimation for electric vehicle with in-wheel motors,” in *Vehicle Power and Propulsion Conference*, 2012, pp. 1286–1291.

[27] X. Huang and J. Wang, “Model predictive regenerative braking control for lightweight electric vehicles with in-wheel motors,” *Proc. Inst. Mech. Eng. Part D J. Automob. Eng.*, vol. 226, no. 9, pp. 1220–1232, Apr. 2012.

[28] Y. Chen, X. Li, C. Wiet, and J. Wang, “Energy Management and Driving Strategy for In-Wheel Motor Electric Ground Vehicles with Terrain Profile Preview,” *IEEE Trans. Ind. Informatics*, no. c, pp. 1–1, 2013.

[29] K. a. Danapalasingam, “Electric vehicle traction control for optimal energy consumption,” *Int. J. Electr. Hybrid Veh.*, vol. 5, no. 3, p. 233, 2013.

[30] H. Fujimoto and S. Egami, “Range extension control system for electric vehicles based on front and rear driving force distribution considering load transfer,” *2011-37th Annu. Conf. IEEE*, pp. 3852–3857, 2011.

[31] L. Laine and J. Fredriksson, “Coordination of Vehicle Motion and Energy Management Control Systems for Wheel Motor Driven Vehicles,” *2007 IEEE Intell. Veh. Symp.*, pp. 773–780, Jun. 2007.

[32] Y. Chen and J. Wang, “A Global Optimization Algorithm for Energy-Efficient Control Allocation of Over-Actuated Systems,” pp. 5300–5305, 2011.

[33] Y. Chen and J. Wang, “Energy-Efficient Control Allocation with Applications on Planar Motion Control of Electric Ground Vehicles,” pp. 2719–2724, 2011.

[34] Y. Chen and J. Wang, “Fast and Global Optimal Energy-Efficient Control Allocation With Applications to Over-Actuated Electric Ground Vehicles,” *IEEE Trans. Control Syst. Technol.*, pp. 1–10, 2011.

[35] Y. Chen and J. Wang, “An adaptive energy-efficient control allocation on planar motion control of electric ground vehicles,” *IEEE Conf. Decis. Control Eur. Control Conf.*, pp. 8062–8067, Dec. 2011.

[36] Y. Chen and J. Wang, “Design and Evaluation on Electric Differentials for Overactuated Electric Ground Vehicles With Four Independent In-Wheel Motors,” *IEEE Trans. Veh. Technol.*, vol. 61, no. 4, pp. 1534–1542, May 2012.

[37] D. P. Bertsekas, *Dynamic Programming and Optimal Control: Volume II*. Athena Scientific, 2007, p. 445.

[38] C. Lin, H. Pengl, J. W. Grizzle, and H. Peng, “A Stochastic Control Strategy for Hybrid Electric Vehicles,” pp. 4710–4715, 2004.

[39] S. J. Moura, H. K. Fathy, D. S. Callaway, and J. L. Stein, “A Stochastic Optimal Control Approach for Power Management in Plug-In Hybrid Electric Vehicles,” pp. 1–11, 2010.

[40] H. Zhang, Y. Qin, X. Li, X. Liu, and M. Engineering, “Driver-Oriented Optimization of Power Management in Plug-In Hybrid Electric Vehicles,” in *EIC Climate Change Technology Conference*, 2013, no. 1569730735, pp. 1–12.

[41] D. F. Opila, R. McGee, J. a. Cook, and J. W. Grizzle, “Performance comparison of hybrid vehicle energy management controllers on real-world drive cycle data,” *2009 Am. Control Conf.*, pp. 4618–4625, 2009.

[42] V. Schwarzer, R. Ghorbani, and R. Rocheleau, “Drive cycle generation for stochastic optimization of energy management controller for hybrid vehicles,” *2010 IEEE Int. Conf. Control Appl.*, pp. 536–540, Sep. 2010.

[43] R. Vijayagopal, L. Michaels, A. P. Rousseau, S. Halbach, and N. Shidore, “Automated Model Based Design Process to Evaluate Advanced Component Technologies,” Apr. 2010.

[44] N. Kim and A. Rousseau, “Comparison between Rule - Based and Instantaneous Optimization for a Single – Mode , Power - Split HEV,” vol. 1, pp. 1–10, 2011.

[45] H. B. Pacejka and E. Bakker, “The Magic Formula Tyre Model,” *Veh. Syst. Dyn.*, vol. 21, no. sup001, pp. 1–18, Jan. 1992.

[46] R. Wang, Y. Chen, D. Feng, X. Huang, and J. Wang, “Development and performance characterization of an electric ground vehicle with independently actuated in-wheel motors,” *J. Power Sources*, vol. 196, no. 8, pp. 3962–3971, Apr. 2011.

[47] J. W. Grizzle, “Power management strategy for a parallel hybrid electric truck,” *IEEE Trans. Control Syst. Technol.*, vol. 11, no. 6, pp. 839–849, Nov. 2003.